Journal of Sedimentary Research

Journal of Sedimentary Research, 2010, v. 80, 791–807
Research Article
DOI: 10.2110/jsr.2010.071

ACOUSTIC PROPERTIES OF ANCIENT SHALLOW-MARINE CARBONATES: EFFECTS OF DEPOSITIONAL ENVIRONMENTS AND DIAGENETIC PROCESSES (MIDDLE JURASSIC, PARIS BASIN, FRANCE)

BENJAMIN BRIGAUD,*[1,2] BENOIT VINCENT,[3] CHRISTOPHE DURLET,[1] JEAN-FRANÇOIS DECONINCK,[1] PHILIPPE BLANC,[4] AND ALAIN TROUILLER[2]

[1]*Université de Bourgogne, UMR CNRS 5561 Biogéosciences, 6 bd Gabriel, 21000 Dijon, France*
[2]*Andra, 1-7 rue Jean Monnet, 92298 Châtenay–Malabry Cedex, France*
[3]*Cambridge Carbonates, Ltd, 14 rue du mont 52320 Marbéville, France*
[4]*Lithologie Bourgogne, 21 rue de l'ingénieur Bertin, 21600 Longvic, France*
e-mail: benjamin.brigaud@u-bourgogne.fr

ABSTRACT: **Examination of petrophysical properties (acoustic velocity, porosity, permeability, and density) and petrographical characteristics (texture, facies composition, and diagenesis) of more than 250 core plugs from the Middle Jurassic carbonates of the eastern Paris Basin provides insights into the parameters controlling acoustic velocities in relatively low-porosity carbonate rocks ($\Phi < 20\%$). The pore-type observations reveal distinct acoustic velocities in samples with intergranular macropores and samples with micropores in subhedral micrite, such that velocities in microporous mudstone–wackestone (lagoonal) deposits are greater than in macroporous grainstone (shoal) samples, at a given porosity range (15–20%). The standard Wyllie and Raymer transforms fit very well with the linear regression between acoustic velocity and porosity from mudstone or lagoonal facies. Marls and fine-grained deposits interpreted as lagoonal facies include statistically significant correlation ($r = 0.9$) between velocity and porosity. However, the data suggest that the wide scatter in velocity–porosity relationship from grainstones are not the result of different sorting, grain size, pore type, dolomite content, or clay content. Instead, early cementation greatly influences acoustic properties during diagenesis, and are interpreted to account for the high variability of velocities over a given porosity range. Specifically, at a given porosity, acoustic velocities in compacted grainstone that did not undergo early cementation are higher than in early-cemented grainstone.**

Petrographic observations suggest that early cementation limits mechanical compaction, creating a heterogeneous medium from the earliest stages of diagenesis (non-touching grains, preservation of intergranular macropores that are partially to totally filled by later blocky calcite cement). The abundant interfaces between micritized ooids, early cement fringes, and blocky calcites in grainstones may induce significant wave attenuation. As a result, the standard time-average equations fail to predict the effect of diagenetic features such as early cementation on sonic velocity. Conversely, an absence of early cementation favors mechanical compaction, grain-to-grain contact, and suturing. The result is a homogeneous micritized grain-supported network that may facilitate wave propagation.

Through demonstration of the key role of early cementation in the explanation of variability in acoustic properties, the results of this study illustrate the complicated factors influencing velocity transforms in carbonates (Wyllie and Raymer), i.e., classical tools for predicting reservoir properties. These insights on the interpretation of Vp and the refinement of velocity–porosity transforms in grainstone units may be broadly applicable to enhancing seismic-based exploration in carbonate successions.

INTRODUCTION

Seismic reflectors result from variations in acoustic impedance, which is the product of sonic velocity and bulk density. In relatively pure carbonate successions, because density variations are relatively small, rock velocity is a key parameter for better constraining the origin of reflection patterns on seismic sections. Wyllie et al. (1956, 1958), Gardner et al. (1974), and Raymer et al. (1980) have investigated the primary factors controlling acoustic velocity in siliciclastic and carbonate rocks, and demonstrated that porosity is a crucial factor. These studies have derived empirical equations such as the "time-average equation" (velocity–porosity transform). With these transforms, impedance data from seismic data can be used to predict porosity distribution, used for modeling hydrocarbon reservoirs (Bashore et al. 1994; Robinson et al. 2008). These relationships are extracted mostly from siliciclastic data sets, but over the last decade or so, several studies have identified parameters controlling velocity–porosity transforms in carbonate strata (Anselmetti and Eberli 1993; Kenter et al. 1997a; Kenter et al. 2002; Kenter et al. 2007; Verwer et al. 2008; Weger et al. 2009). These studies demonstrate that the complex diagenetic alteration pathways in carbonate rocks explain the wide range of velocity values at a given porosity, i.e., the wide scattering of data evident in porosity–velocity transforms. In these systems, diagenetic phenomena such as early cementation, burial cementation, compaction, dissolution, and dolomitization control the

* Present Address: Université de Paris Sud, UMR CNRS 8148 IDES, Bâtiment 504, 91405 Orsay Cedex, France

 1527-1404/10/080-791/$03.00

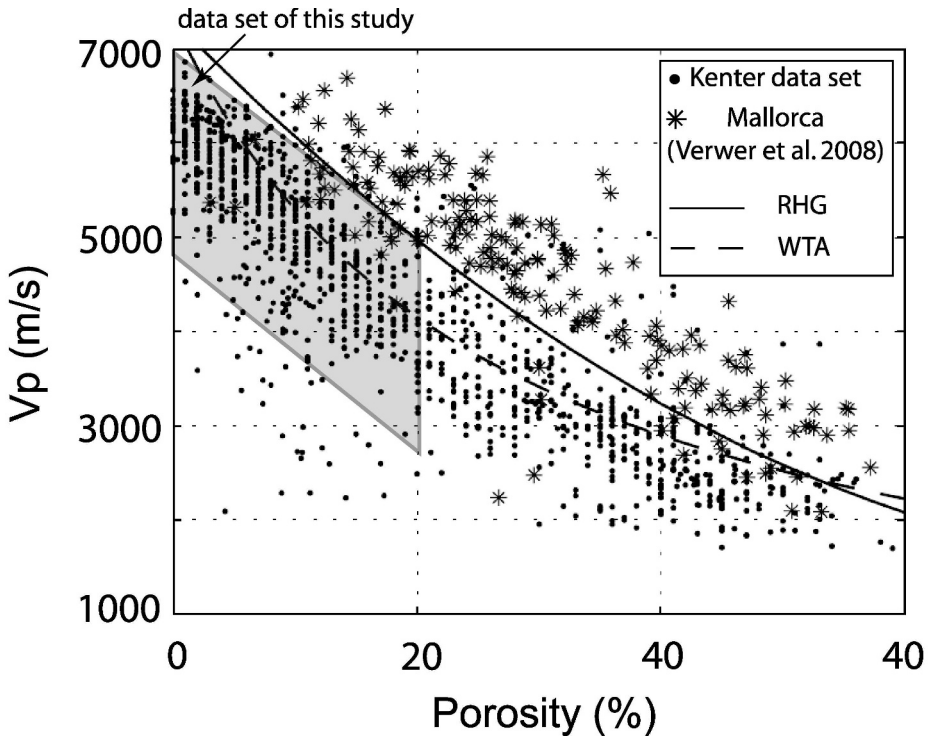

FIG. 1.—Velocity–porosity transform in carbonate, comparing the data set of our study with data from the literature (Verwer et al. 2008). WTA, Wyllie time-average equation for calcite; RHG, Raymer equation for calcite.

evolution of rock fabric, pore space, and pore type, the latter being key parameters to understand the acoustic properties of carbonates (Anselmetti and Eberli 1993; Kenter et al. 1997a; Kenter et al. 2002; Baechle et al. 2008; Fournier and Borgomano 2009; Weger et al. 2009). Since this realization, numerous case studies have focused on highly porous ($\Phi > 15\%$) relatively young (Cenozoic) carbonates (Anselmetti and Eberli 1993; Anselmetti et al. 1997; Anselmetti and Eberli 2001; Kenter et al. 2002; Verwer et al. 2008; Verwer and Braaksma 2009) or ancient carbonates (Carboniferous, Permian, Middle Jurassic, and Cretaceous strata) (Rafavich et al. 1984; Kenter et al. 1997a; Kenter et al. 1997b; Assefa et al. 1999; Kenter et al. 2001; Assefa et al. 2003; Røgen et al. 2005; Braaksma et al. 2006; Weger et al. 2009). Investigations of highly cemented, ancient carbonates with low porosity ($\Phi < 15\%$) are less common, however (Fig. 1).

To explore controls on petrophysical properties of low–porosity carbonates, this study reports on examination of about 250 petrophysical samples from the Middle Jurassic carbonates of the Paris Basin, focusing on the role of cement types and especially of early cements in grainstone on acoustic velocity. Middle Jurassic carbonates of the eastern part of the Paris Basin are extensively cemented, with low porosity and permeability ($\Phi < 15\%$ and $K < 0.05$ mD). Specifically, this study investigates (1) the power of the existing velocity transform on recognition of texture, depositional facies, and/or diagenesis, and (2) the influence of both depositional environment characteristics (texture, clay content, grain size, and sorting) and diagenetic alterations (early cementation, compaction, blocky calcite burial cementation) on acoustic velocity. The results of this study provide new insights about the behavior of acoustic velocity in cemented limestone, improving the knowledge of the relationships among petrophysics (sonic velocity and porosity) and early diagenetic processes (cementation and mechanical compaction).

GEOLOGICAL SETTING

The Middle Jurassic of the eastern Paris Basin consists of carbonate and marl deposits (Fig. 2A), and is well–known in terms of depositional environment and diagenetic characteristics (Guillocheau et al. 2002; Buschaert et al. 2004; Brigaud et al. 2009a; Brigaud et al. 2009b). During the Bajocian–Callovian interval, the Paris Basin was an epicontinental sea located at subtropical latitudes (28–32° N) and open to the Atlantic, Tethys, and Northern Oceans (Fig. 2B); (Contini and Mangold 1980; Thierry and Barrier 2000). The early Bajocian limestones are composed mainly of bioclastic calcarenites and coral buildups (the Calcaires à polypiers; Fig. 2C) that were deposited on a vast intracratonic carbonate platform (Durlet and Thierry 2000; Brigaud et al. 2009a). The Late Bajocian Marnes de Longwy and Oolite miliaire (75 m thick) comprise aggrading and prograding marls and oo–bioclastic deposits that represent a ramp dipping gently southwards from the London–Brabant landmass. During the Bathonian, three main depositional environments are recognized (Fig. 2C) (Purser 1967, 1975, 1989; Gaumet et al. 1996; Gaumet et al. 2001; Brigaud et al. 2009a): (1) a typical platform barrier environment with abundant ooids (Oolite Blanche and Oolite de Fréville); (2) behind the barrier, a protected lagoon with fine sedimentation characterized by mudstone facies with oncoids and large benthic foraminifera (Calcaires de Chaumont and Calcaires de Neufchâteau); and (3) a more proximal lagoon setting with supratidal to intertidal muds (fenestral structures and stromatolites) and intraclastic washover deposits that formed low islands bordered by beachrock (Purser 1975). Early Callovian carbonates, confined to the southeastern part of the study area (Pierre de Dijon-Corton and Pierre de Ladoix; Fig. 2C), displays mainly ooids, bryozoans, and bivalve-rich calcarenites.

A detailed sedimentological and stratigraphic study of the Middle Jurassic of this part of the Paris Basin has been carried out on cores drilled by the French National Agency for Radioactive Waste Management (Andra), and the reader should refer to the recent resulting papers for more detailed information (e.g., Brigaud et al. 2009a). This succession is of primary importance because these carbonate formations form the basement of the natural clay barrier chosen by the French National Agency for Radioactive Waste Management (Andra) as a target for a natural laboratory to study the feasibility of future deep disposal of radioactive wastes. As seismic lines are available across this part of the Paris Basin,

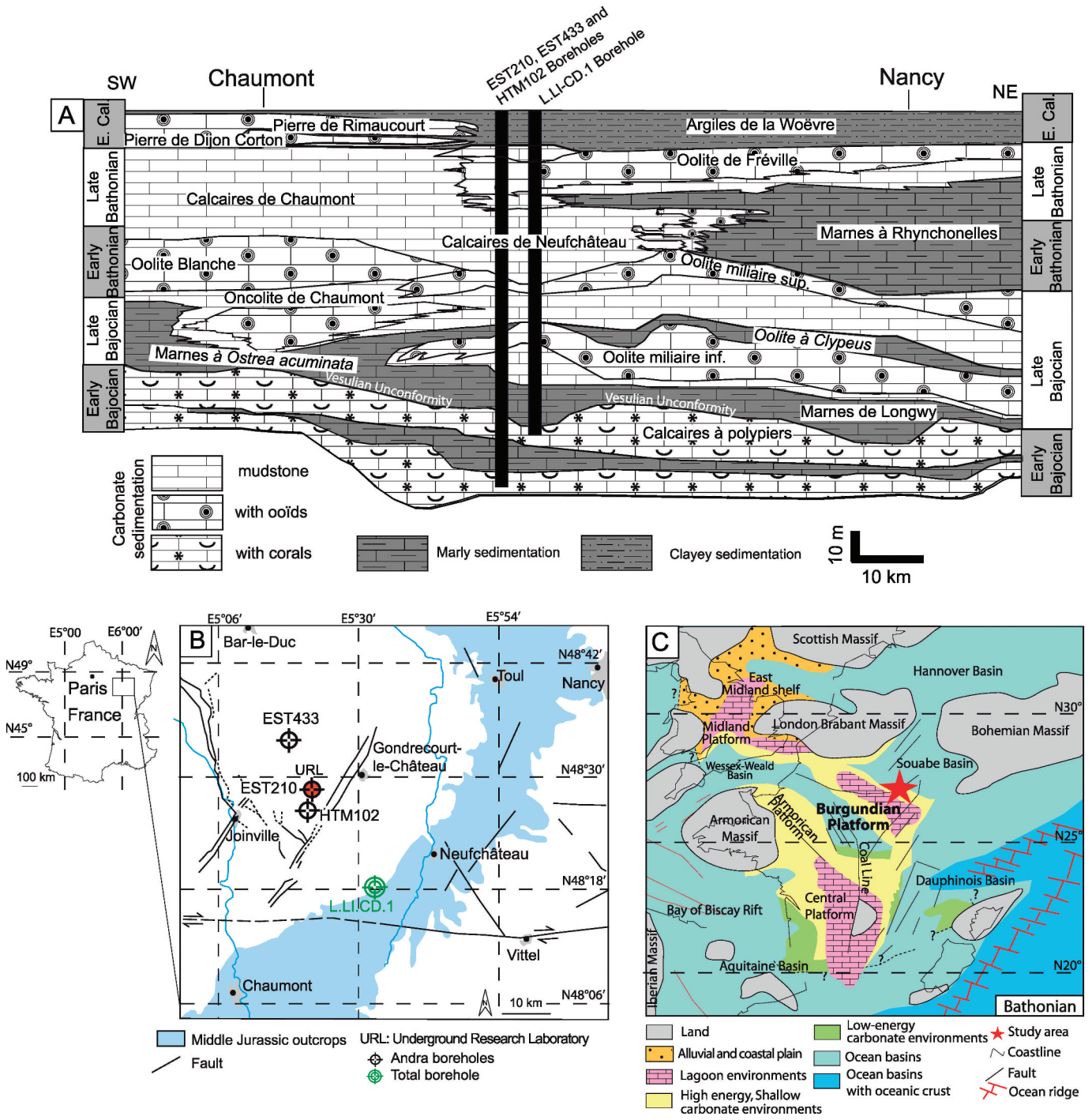

FIG. 2.—**A)** Schematic NE–SW transect illustrating the lithostratigraphic architecture during the Bajocian–Early Callovian interval (modified from Brigaud et al. 2009a, b). **B)** Location of the four study cores in the eastern part of the Paris Basin (Lorraine and Champagne–Ardennes regions) on a simplified geological map (modified from Brigaud et al. 2009a, b). **C)** Paleogeographic map of the Bathonian (modified after Purser 1975; Enay and Mangold 1980; Thierry and Barrier 2000).

constraining the physical causes of seismic reflectors in these carbonates is crucial for geologists and hydrologists who aim to use these seismic data to accurately illustrate the porosity distribution in these strata. In addition, the Middle Jurassic limestones are currently studied as (1) potential targets for CO_2 storage (Sterpenich et al. 2009), (2) a possible geothermal resource (Menjoz et al. 1992), and finally (3) residual minor oil reservoirs (Granier 1995; Mougenot 1999; Wendebourg and Lamiraux 2002).

METHODS

Laboratory Data

Samples described in this study come from four cores of the Eastern Paris Basin: EST210, EST433, HTM102, and L.LI.CD.001 (Fig. 2A). Collectively, these cores capture the range of variability in depositional and diagenetic character.

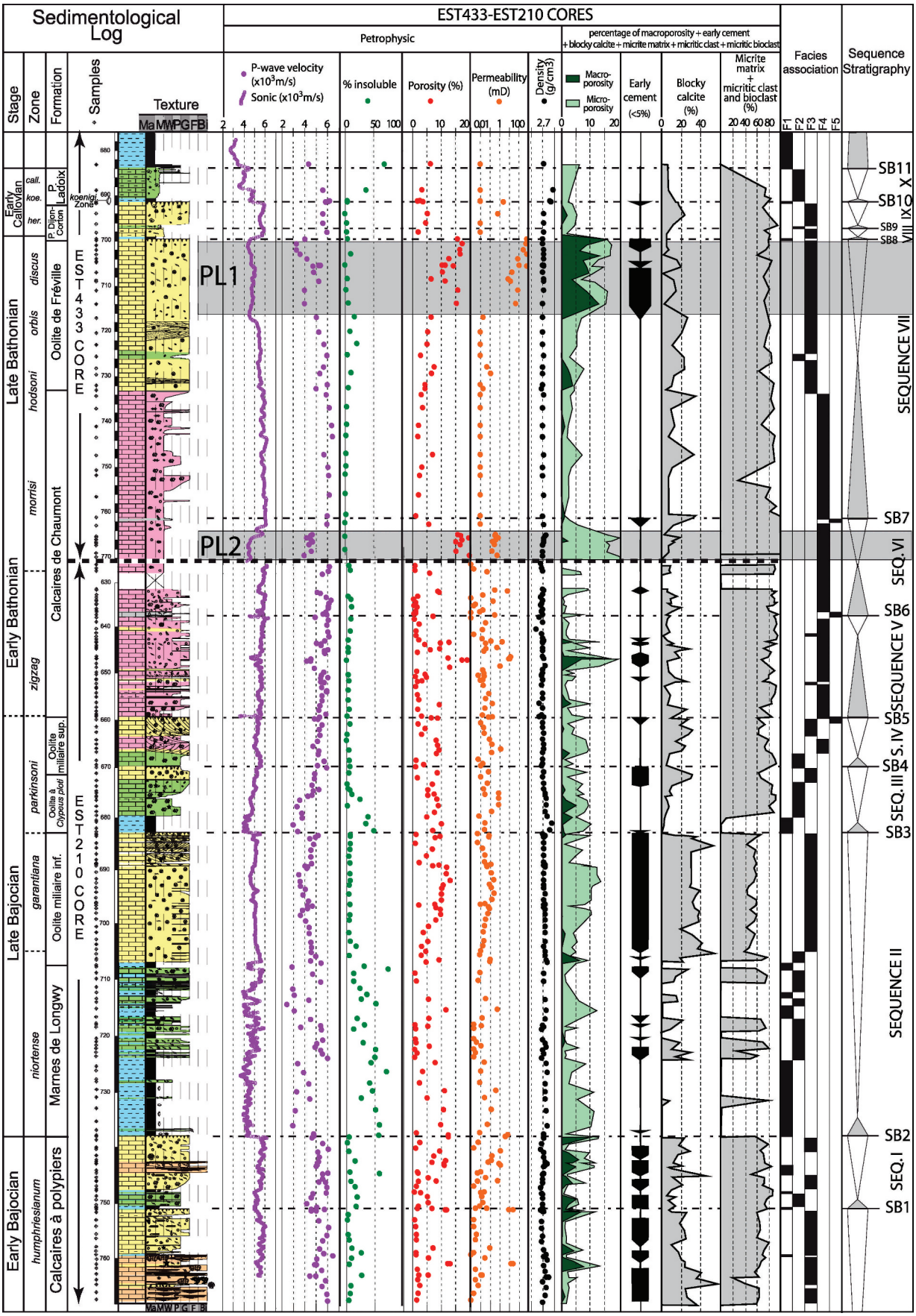
Sedimentological Log
EST433-EST210 CORES
Petrophysic
percentage of macroporosity + early cement + blocky calcite + micrite matrix + micritic clast + micritic bioclast
Stage
Zone
Formation
Samples
Texture
P-wave velocity (x10³m/s)
Sonic (x10³m/s)
% insoluble
Porosity (%)
Permeability (mD)
Density (g/cm3)
Macro-porosity
Micro-porosity
Early cement (<5%)
Blocky calcite (%)
Micrite matrix + micritic clast and bioclast (%)
Facies association
Sequence Stratigraphy
Early Callovian
Late Bathonian
Early Bathonian
Late Bajocian
Early Bajocian
Ladoix
P. Dijon-Corton
Oolite de Fréville
Calcaires de Chaumont
Oolite miliaire sup.
Oolite à Clypeus ploti
Oolite miliaire inf.
Marnes de Longwy
Calcaires à polypiers
koenigi Zone
EST433 CARBONATE RAMP
EST210 CARBONATE RAMP
PL1
PL2
SB11
SB10
SB9
SB8
SB7
SB6
SB5
SB4
SB3
SB2
SB1
SEQUENCE VII
SEQ. VI
SEQUENCE V
S. IV
SEQ. III
SEQUENCE II
SEQ. I

Acoustic Velocity, Porosity, Permeability, and Grain Density

Acoustic velocity was measured on 262 one-inch (2.54 cm) plugs drilled using a water-cooled diamond coring drill and oriented vertically with respect to the bedding. All plugs were cut to a maximum length of 8 cm, and part of each was used to make a thin section. The samples were dried in an oven at 60 °C for 72 hours and equilibrated at ambient temperature and humidity before measurement. Ultrasonic compressional (P-wave) velocities were measured with a transducer that propagated the compressional waves along the plug axis. During the measurement, a compression was applied and a coupling fluid was used to maintain a good contact between transducers and plugs. Ultrasounds were produced under 500 kHz, and the precision of velocity measurements in these data sets is about 1.25%.

Porosity and permeability were measured on 251 of the plugs at Panterra Laboratory, Leiderdorp (The Netherlands). Porosity of dry samples was measured by the helium expansion method at ambient temperature and pressure. Permeability tests were performed with an unsteady-state air permeameter (lower limit of 0.001 mD) for 176 samples (EST210 and HTM102 cores) and on a steady-state permeameter (lower limit of 0.01 mD) for the other 75 samples (EST433 and L.LI.CD.001). The 251 air-permeability measurements were made at a confining pressure of 400 psi, including the Klinkenberg slip factor. Grain density, the ratio of the plug weight to its grain volume, is deduced with the helium porosity measurement in plug.

Detailed Petrography and Diagenesis

Thin sections were impregnated with blue epoxy to visualize the pore space. Thin sections were prepared from all measured plugs, and microfacies were analyzed for a total of 266 thin sections. Texture and grain compositions were estimated from these thin sections. Diagenetic features are described in detail in Brigaud et al. (2009b).

Carbonate content was measured on cuttings during drilling with a 2 m sample interval. The samples analyzed for carbonate content during drilling do not correspond exactly to the plug sampling, but the interval between a plug and a $CaCO_3$ value is invariably less than 1 m. Sample powders were reacted with acid (HCl), and a pressure sensor measured CO_2 volume after 1 minute to determine the calcite percentage and after 15 minutes to determine the dolomite and insoluble percentages.

In the present study, composition was detailed on a restricted set of 229 thin sections (excluding marls) by point-counting quantification of micritic grains (ooids, peloids, pellets, oncoids, bioclasts), micrite matrix, blocky calcite cement, early calcite fringe, recrystallized bioclasts, and macroporosity, using JmicroVision Image analysis software, with a minimum of 100 counts per thin section, and expressed in percentage (Roduit 2008); (Figs. 3, 4). The term micrite is used in a nongenetic descriptive sense (Loreau 1972) for a limestone composed of calcite microcrystals (crystal size < 4 μm). Here micrite defines both the fine crystalline matrix of limestone and the fine crystalline constituent of carbonate grains. Micrite content in sample is then the addition of microcrystalline matrix, micritic clasts, and micritized bioclasts (Figs. 2, 3). Microporosity was estimated as the difference between measured helium porosity and macroporosity estimated by point counting. Finally, grain size was measured from grainstone samples only ($n = 107$) along the longest axis of 150 grains within a rectangle window and mean grain size and sorting (one standard deviation of grain size, Melzer and Budd 2008) were calculated.

Wireline Logs

The sonic log corresponds to average velocity measured over several meters from the borehole and at lower frequency (10 kHz) than the discrete measurement on core plugs at higher frequency (500 kHz). This difference in the scale of investigation can be important when attempting to explicitly compare velocity data from different sources (Bourbié et al. 1986; Kenter and Ivanov 1995; Kenter et al. 2002; Zinszner and Pellerin 2007).

RESULTS

The raw environmental and petrophysical data (Appendix) are available in the JSR data archive online (see Acknowledgments section).

Petrophysical Properties

Measured P-wave velocities ($n = 262$) range from 2460 to 6477 m/s (Figs. 3, 4). In the EST433 core, Vp values are high (about 6000 m/s) in mudstone–packstone of the Bathonian Calcaires de Chaumont and in grainstone of the Bajocian Calcaires à polypiers (Fig. 3). Velocities are low in the upper part of the Oolite de Fréville in EST433 core (Porous Level 1: PL1 with $\phi > 15\%$ and Vp = 3000–4000 m/s; Fig. 3), where the dominant texture is grainstone and in the middle interval of the fine limestone of the Calcaires de Chaumont (Porous layer 2: PL2 with $\phi > 15\%$ and Vp = 4000–5000 m/s). Samples of the Calcaires de Chaumont of EST210 core also exhibit high velocities (about 6000 m/s; Fig. 3). Velocity decreases in the Oolite miliaire (3000 to 5000 m/s) and reaches very low values in the Marnes de Longwy and Oolite à *Clypeus ploti* ($<$ 3000 m/s; Figs. 3, 4). Along the HTM102 core, the P-wave velocity appears relatively homogeneous (5000 to 5500 m/s; Fig. 3). Velocity ranges from 5000 to 6000 m/s along the L.LI.CD.001 core.

Porosity displays a wide range of values from 0.4% to 19.9%, with a mean value of 6.0% and a standard deviation of 4.6%. However, the median value is 5.1%, and 80% of the samples ($n = 251$) include less than 10% porosity (Fig. 5).

Permeabilities are also very low, with a median value of 0.03 mD. Eighty percent of the samples ($n = 251$) are below 0.16 mD. High permeabilities occur only in PL1, with a maximum value of 690 mD (Fig. 5). This layer corresponds to a water flux in the well (transmissivity of $10^{-4}m^2/s$; Scholz and Garry 2009).

Density ranges between 2.3 g/cm^3 and 2.9 g/cm^3 with a mean value of 2.7 g/cm^3 and a standard deviation of 0.04 g/cm^3. The extraordinary homogeneity of the laboratory density values at 2.7 g/cm^3 along the EST433 and EST210 cores (Fig. 3) is noteworthy, emphasizing the key role of velocity in impedance calculations in many carbonates.

Quantitative Petrography and Facies Associations

Five facies associations (F1 to F5) were defined from the Bajocian–Callovian succession exposed in the eastern part of the Paris Basin (Brigaud et al. 2009a), representing five major depositional environments from distal to proximal environments along a ramp (Brigaud et al. 2009a). F1 is represented mainly by heavily bioturbated marls with quartz, bivalves, echinoderms, and clay content of about 45%. This facies association is interpreted as being deposited in an outer-ramp setting below storm wave base (lower offshore). F2 consists of oncoid grainstone to wackestone including bivalves and echinoderms, with an average clay content of about 20%. It corresponds to an upper offshore environment,

←

FIG. 3.—Sedimentological log of the Middle Jurassic limestone from EST210 and EST433 cores, with P-wave velocity from plugs, sonic, insoluble content, helium porosity, air permeability, and grain density. Proportions of macroporosity, early cement, blocky calcite, micrite matrix, micritic clast, and micritic bioclast, are expressed in percentage. Facies associations and sequence stratigraphy after Brigaud et al. (2009a). PL: porous level.

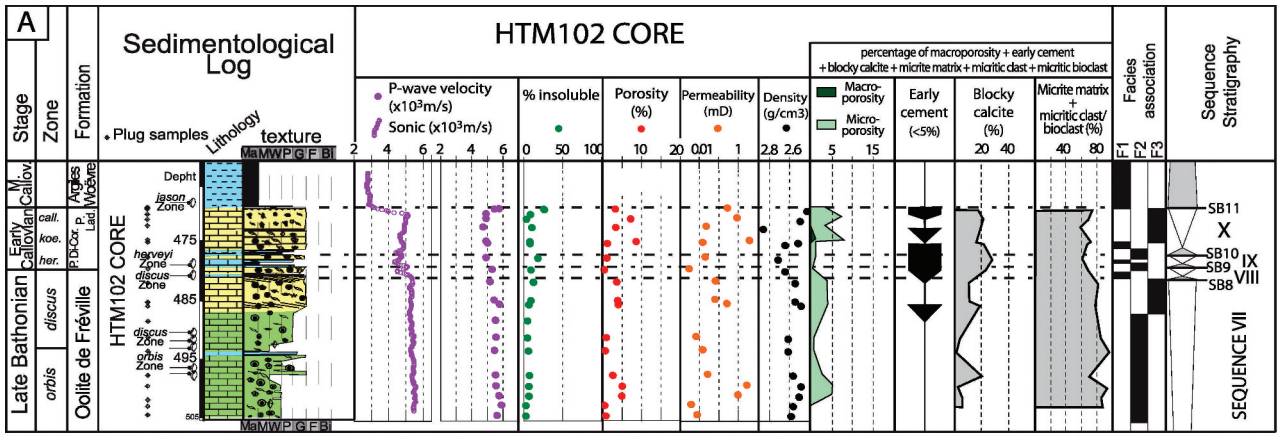
A
Sedimentological Log
HTM102 CORE
Plug samples
Lithology
texture
P-wave velocity (x10³m/s)
Sonic (x10³m/s)
% insoluble
Porosity (%)
Permeability (mD)
Density (g/cm3)
percentage of macroporosity + early cement + blocky calcite + micrite matrix + micritic clast + micritic bioclast
Macro-porosity
Micro-porosity
Early cement (<5%)
Blocky calcite (%)
Micrite matrix + micritic clast/ bioclast (%)
Facies association
Sequence Stratigraphy
Late Bathonian
Early Callovian
M. Callov.
Oolite de Fréville
HTM102 CORE
SB11
SB10
SB9
SB8
SEQUENCE VII

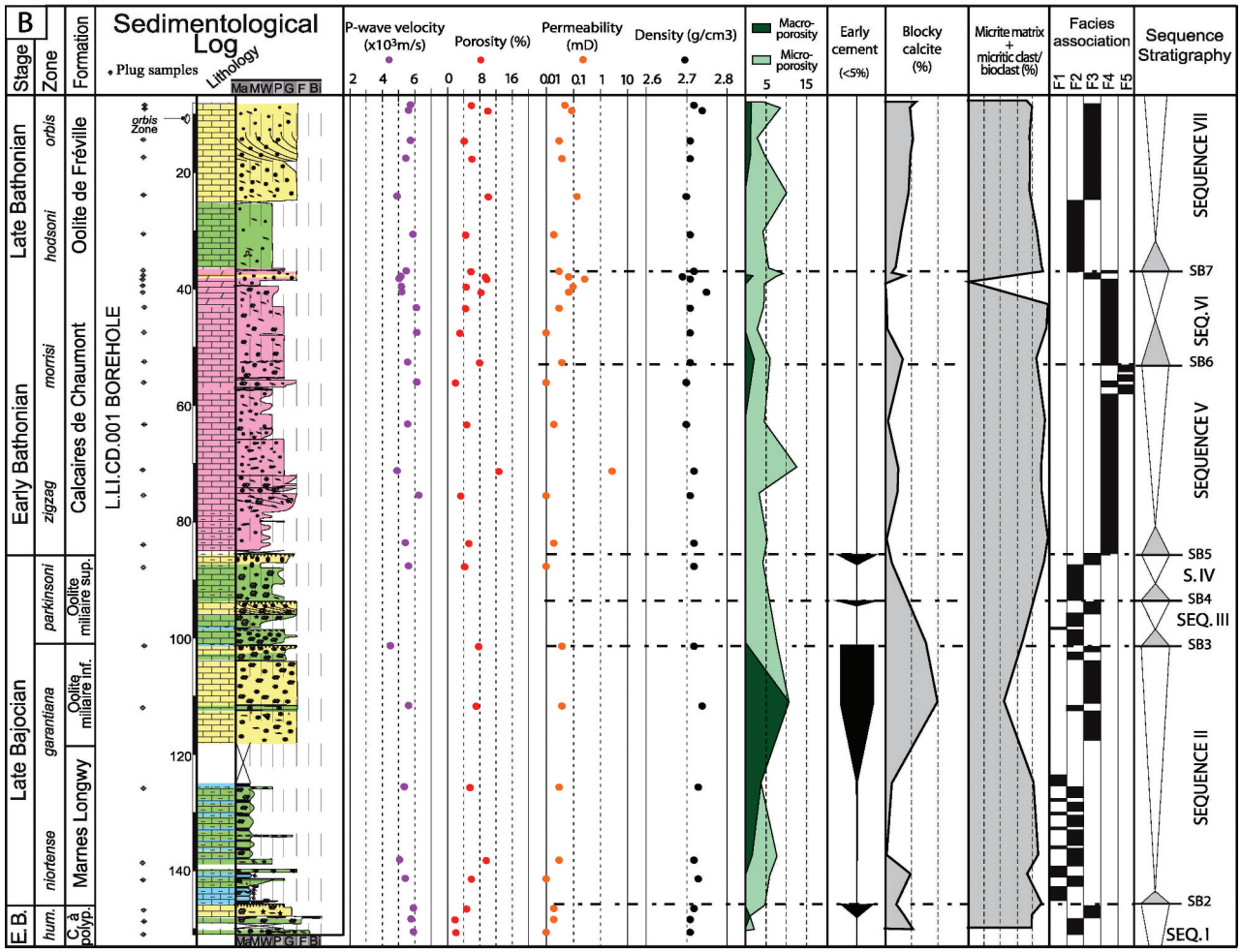
B
Sedimentological Log
L.LI.CD.001 BOREHOLE
Plug samples
Lithology
P-wave velocity (x10³m/s)
Porosity (%)
Permeability (mD)
Density (g/cm3)
Macro-porosity
Micro-porosity
Early cement (<5%)
Blocky calcite (%)
Micrite matrix + micritic clast/ bioclast (%)
Facies association
Sequence Stratigraphy
Late Bathonian
Early Bathonian
Late Bajocian
E.B.
Oolite de Fréville
Calcaires de Chaumont
Oolite miliaire sup.
Oolite miliaire inf.
Marnes Longwy
SB7
SB6
SB5
SB4
SB3
SB2
SEQUENCE VII
SEQ. VI
SEQUENCE V
S.IV
SEQ. III
SEQUENCE II
SEQ.I

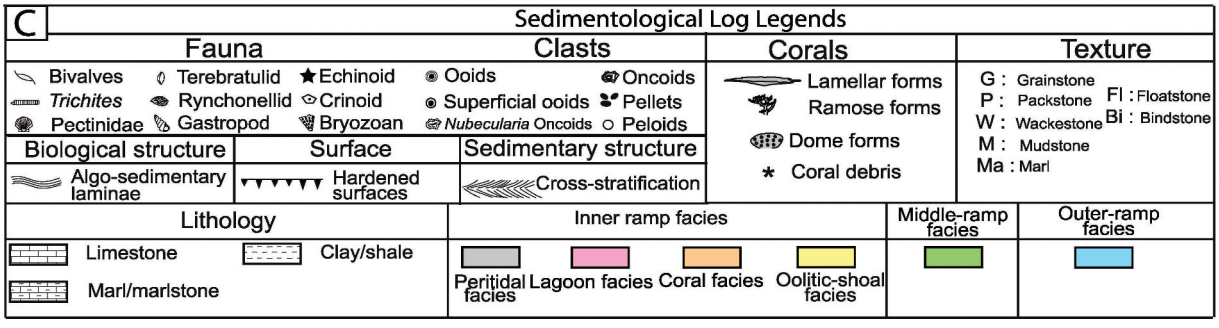
C
Sedimentological Log Legends
Fauna
Bivalves
Terebratulid
Echinoid
Trichites
Rynchonellid
Crinoid
Pectinidae
Gastropod
Bryozoan
Clasts
Ooids
Oncoids
Superficial ooids
Pellets
Nubecularia Oncoids
Peloids
Corals
Lamellar forms
Ramose forms
Dome forms
Coral debris
Texture
G : Grainstone
P : Packstone
W : Wackestone
M : Mudstone
Ma : Marl
Fl : Floatstone
Bi : Bindstone
Biological structure
Algo-sedimentary laminae
Surface
Hardened surfaces
Sedimentary structure
Cross-stratification
Lithology
Limestone
Clay/shale
Marl/marlstone
Inner ramp facies
Peritidal facies
Lagoon facies
Coral facies
Oolitic-shoal facies
Middle-ramp facies
Outer-ramp facies

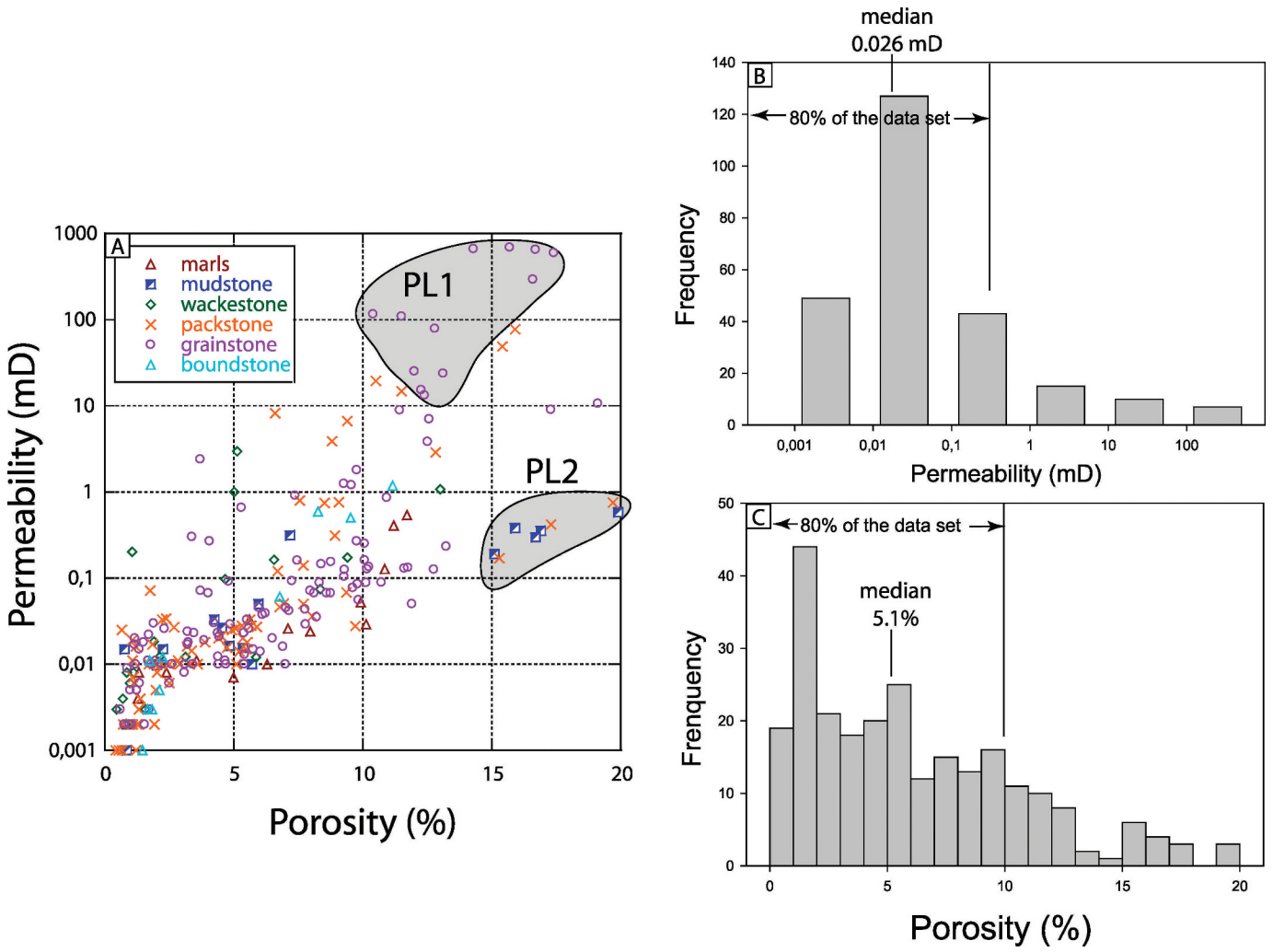

FIG. 5.—**A)** Porosity–permeability analyses in cores from Middle Jurassic limestones in Eastern Paris Basin, sorted by texture (cores EST210, EST433, HTM102, and L.Li.CD.001). **B)** Frequency distribution of plug permeability (80% of the data set is lower than 0.35 mD). **C)** Frequency distribution of plug porosity (80% of the data set is lower than 10%).

deposited above storm wave base in a mid-ramp setting. F3 is distinguished by ooid-rich grainstone including bivalves, echinoderms, and coral debris, with a clay content of less than 5%. This facies association is interpreted to represent shoreface shoals in an inner-ramp setting. F4 is mudstone to grainstone dominated by oncoids, pellets, and foraminifera with very high carbonate content (about 95%). It corresponds to subtidal to supratidal inner-ramp environments. F5 is composed of oncoids–gastropods, algal laminated stromatolites, and lignite and a few grainstones–rudstones. Collectively, it was interpreted to have been deposited on beaches bordering low washover islands in intertidal to supratidal inner ramp, with local early cementation by meniscus and microstalactitic cements (Purser 1975).

Grainstone is a common texture, representing 46% of the data samples (n = 122). In grainstones, a 15 m-thick layer with permeability of more than 100 mD constitutes an aquifer network (Porous Layer 1, PL1). Grains commonly are micritized (Figs. 6, 7), and micritic ooids, clasts, or micritized bioclasts may represent about 60% of the total facies volume of the inner-ramp setting.

The Porous Layer 2 (PL2) developed within the Calcaires de Chaumont, corresponding to mudstone–wackestone deposits with high microporosity (Figs. 3, 5). SEM observations reveal intercrystalline microporosity in these micritic facies. In this porous level, micrite crystals are subhedral according to the classification by Lambert et al. (2006), contrasting with nonporous mudstone composed of compact anhedral micrite crystals (Fig. 6G, H).

Petrography and Diagenesis

A detailed diagenetic study of the Middle Jurassic limestone revealed a succession of about 10 diagenetic cements that altered their permeability and porosity properties (Brigaud et al. 2009b). The low porosity and permeability of grainstone (ϕ = 7% on average) is related to the

←

FIG. 4.—**A)** Sedimentological log of upper part of the Middle Jurassic limestone from HTM102 cores with P-wave velocity from plugs, sonic, insoluble content, helium-porosity, air-permeability, grain density, facies associations, and sequence stratigraphy (after Brigaud et al. 2009a). **B)** Sedimentological log of the Middle Jurassic limestone from L.Li.CD.001. **C)** Key to the sedimentological log and geochemical values.

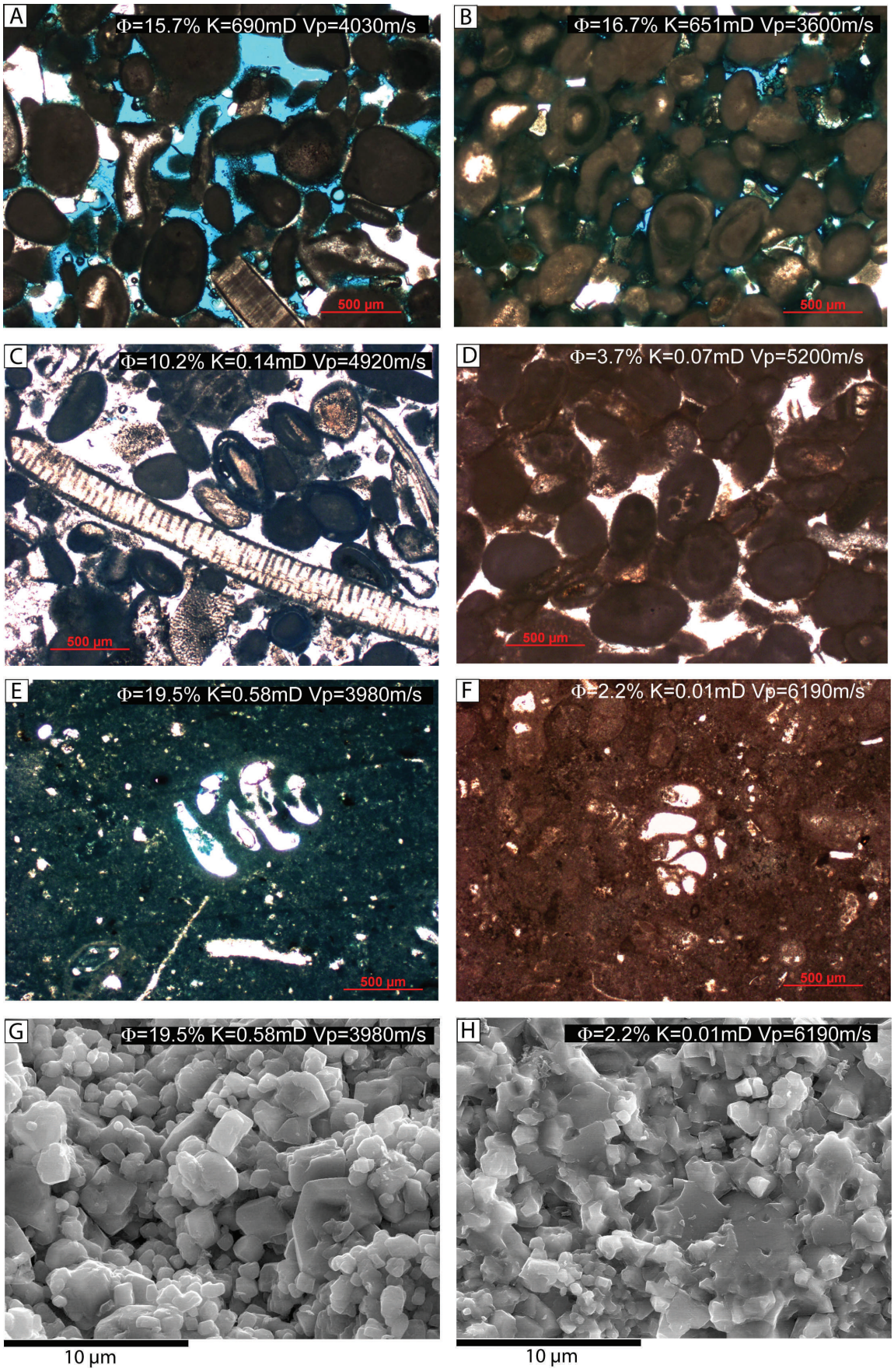
A
Φ=15.7% K=690mD Vp=4030m/s
500 µm
B
Φ=16.7% K=651mD Vp=3600m/s
500 µm
C
Φ=10.2% K=0.14mD Vp=4920m/s
500 µm
D
Φ=3.7% K=0.07mD Vp=5200m/s
500 µm
E
Φ=19.5% K=0.58mD Vp=3980m/s
500 µm
F
Φ=2.2% K=0.01mD Vp=6190m/s
500 µm
G
Φ=19.5% K=0.58mD Vp=3980m/s
10 µm
H
Φ=2.2% K=0.01mD Vp=6190m/s
10 µm

extensive development of blocky low-magnesium calcite (LMC) cement. In grainstone, blocky calcite cement can represent up to 40% of the sample volume. Three blocky calcite zones represent about 80% of the total cement volume (Brigaud et al. 2009b). An exception is the porous layer (PL1) at the top of the Oolite de Fréville, which consists of a poorly cemented grainstone composed of micritic ooids and bioclasts (Figs. 3, 6, 7). Three zones of blocky calcite (Bc1, Bc2, and Bc3) are present but in minor proportions given the large interparticle pore spaces (Figs. 3, 6, 7).

Four types of early cements occur in grainstones of an inner-ramp setting (Brigaud et al. 2009b), but they rarely constitute more than 5% of the total cement volume. The first type consists of inclusion-free bladed to scalenohedral calcite (Fig. 7A, C, D). The second type consists of inclusion-rich isopachous fibrous calcite (IFC; Fig. 7), and corresponds to recrystallized high-magnesium calcite (HMC) of marine origin. The third type of early cement corresponds to microstalactitic cements, displaying radiaxial to bladed fabrics, and occurring just below the sequence boundary SB7 (Fig. 3). The fourth type corresponds to inclusion-free LMC forming meniscus cements, and occurring just below the sequence boundary SB8 (Figs. 3, 7B).

Sonic-Log Data.—Sonic velocities range from about 2000 m/s in the Callovian–Oxfordian (COX) clays to 6000 m/s in the Pierre de Dijon-Corton, Pierre de Ladoix, the Calcaires de Chaumont, and the Calcaires à polypiers (Fig. 3). Velocities are generally higher in these carbonate formations than in the marl units, except in the two porous levels (PL1, PL2; Fig. 3). Log velocity is inversely correlated with the insoluble content (mainly clays in this study). Sonic logs are consistent with discrete measurements of P-wave velocity measured on plugs.

Factors Controlling Velocity

Facies Association, Texture, and Clay Content

The porosity–Vp plot of all plug samples show a first-order trend of decreasing Vp with increasing porosity (Fig. 8). On a porosity–Vp cross-plot displaying sample textures, mudstone and marls define clear trends (Vp = 5220–1937 log ϕ, r = 0.9 for marls and Vp = 6100–98 ϕ, r = 0.9 for mudstone), whereas grainstone (50% of the whole data set) displays a poorly defined cloud (Fig. 8A). For instance, for a porosity of 10%, Vp for grainstone samples ranges from about 3500 to 5800 m/s. Finally, wackestone and packstone include two subtle trends: the first follows the mudstone data, and a second suite of samples form a steeper slope and reaches the marls transform, probably reflecting an increase in clay content (Fig. 8C). Collectively, these trends are consistent with the results of Anselmetti and Eberli (1993) and Kenter et al. (1997b), who show that, for a given porosity, carbonate minerals have higher velocity than siliciclastic minerals. The standard Wyllie (WTA) and Raymer (RHG) transforms for limestones are plotted with rock matrix and fluid velocities of 6700 m/s and 1520 m/s for Wyllie and RHG transforms, respectively (Fig. 8A).

A cross-plot of porosity versus Vp in which the five facies associations are subdivided reveal distinct trends for each facies (Fig. 8B). The standard Wyllie and RHG transforms fit very well with the linear regression from mudstone (Vp = 6100–98 ϕ, r = 0.9; Fig. 8A) and/or lagoonal facies (Vp = 6098–95 ϕ, r = 0.9; Fig. 8B). Marls, whose clay content exceeds 30%, display the lowest P-wave velocity, and are easily differentiated from limestone by their acoustic properties (Fig. 8C). All the other samples, with clay contents of less than 30%, do not follow a clear porosity–Vp transform, as previously pointed out by Anselmetti and Eberli (1993). No direct correlation between clay content and velocity exists for the entire dataset (Fig. 8C). For example, for porosities around 10% and clay content $\leq$ 5%, velocities range from about 3200 to 6000 m/s. This same characteristic is true for subsets of data as well; a cross-plot of clay content versus velocity clearly shows that there is no correlation between clay content and velocity in the grainstone samples (Fig. 9A). Grainstone displays a wide range of velocities at a given porosity, without clear relationship between Vp and porosity (Fig. 8A), or between dolomite content and velocity (Fig. 9B).

Influence of Pore Type (Microporosity versus Interparticle Macroporosity).—Previous studies have shown that the variability of pore types may explain part of the dispersion of acoustic velocity of carbonates (Anselmetti and Eberli 1993; Anselmetti et al. 1997; Anselmetti and Eberli 2001; Kenter et al. 2002; Weger et al. 2009). In these Middle Jurassic carbonates, pores are mainly composed of (1) microporosity (intermicrite crystals porosity; $<$ 10 µm; Fig. 6G), and (2) interparticle macroporosity (several tens of µm to 5 mm; Fig. 6A). Consequently, pore-typing does not explain the entire variability of Vp in these carbonates, except for the highest porosity (15–20%), where macroporous samples display lower Vp than microporous samples (Fig. 8D) of the same porosity. Thus, the two porous levels PL1 (macroporous and high permeability) and PL2 (microporous and low permeability) can be differentiated by their acoustic velocities, which is locally crucial for the prediction of their distribution.

Influences of Grain Size and Sorting.—Grain size and sorting do not control the velocity–porosity relationships in the Middle Jurassic grainstones of the Paris Basin (Fig. 9C, D). Well-sorted samples display a range of Vp between 3000 to 6200 m/s; similarly, each grain-size class displays wide ranges of Vp values (Fig. 9D).

It is noteworthy that the most porous samples ($>$ 15%) are all fine grained (grain size $<$ 0.4 mm) and well sorted ($>$ 0.2 mm; Fig. 9C, D). These samples correspond to the porous level PL1, developed in oolitic-shoal deposits, which may explain the good sorting, whereas the porosity merely reflects incomplete cementation (cf. Petrography and Diagenesis).

DISCUSSION

Origin of the Wide Range of Acoustic Velocity in Grainstone

The Role of Calcite Cements.—The Middle Jurassic carbonates of the Paris Basin underwent successive cementation phases (Fig. 7). After a minor early synsedimentary cementation (10% of the total cement volume), two extensive blocky calcite cement phases (80% of the total cement volume) developed as a result of meteoric circulation during Early Cretaceous uplift phases (Vincent et al. 2007; Brigaud et al. 2009b). Lateral meteoric water recharges seeped into Middle Jurassic limestones

←

FIG. 6.—Petrographic character of the various facies associations from the Middle Jurassic of the Paris Basin. **A)** Ooid and bioclast grainstone (facies association F3)–Oolite de Fréville, E409 sample, EST433 core, 699.6 m. **B)** Non-cemented ooid grainstone (facies association F3)–Oolite de Fréville, E412 sample, EST433 core, 703 m. **C)** Early-compacted bioclastic and oolitic grainstone (facies association F3) with substantial blocky calcite development. The blue color of micritic bioclasts and ooids indicates microporosity–Oolite de Fréville, CAR5 sample, L.Li.CD.001 core, 23.9 m. **D)** Early-compacted ooid grainstone, with burial cementation (facies association F3)–Oolite de Fréville, HTM011 sample, HTM102 core, 483.3 m. **E)** Microporous mudstone with miliolid foraminifera (facies association F4). This sample characterizes the Porous Level 2 (PL2), Calcaires de Chaumont, E445 sample, EST433 core, 769.9 m. **F)** Mudstone with miliolid foraminifera (facies association F4), Calcaires de Chaumont, E435 sample, EST433 core, 756.5 m. **G)** Detailed microstructure of sample E445 described in Part E. The porous mudstone displays subrounded and subhedral micrite. **H)** Compact micrite. Crystals are anhedral, and microspar indicates cementation.

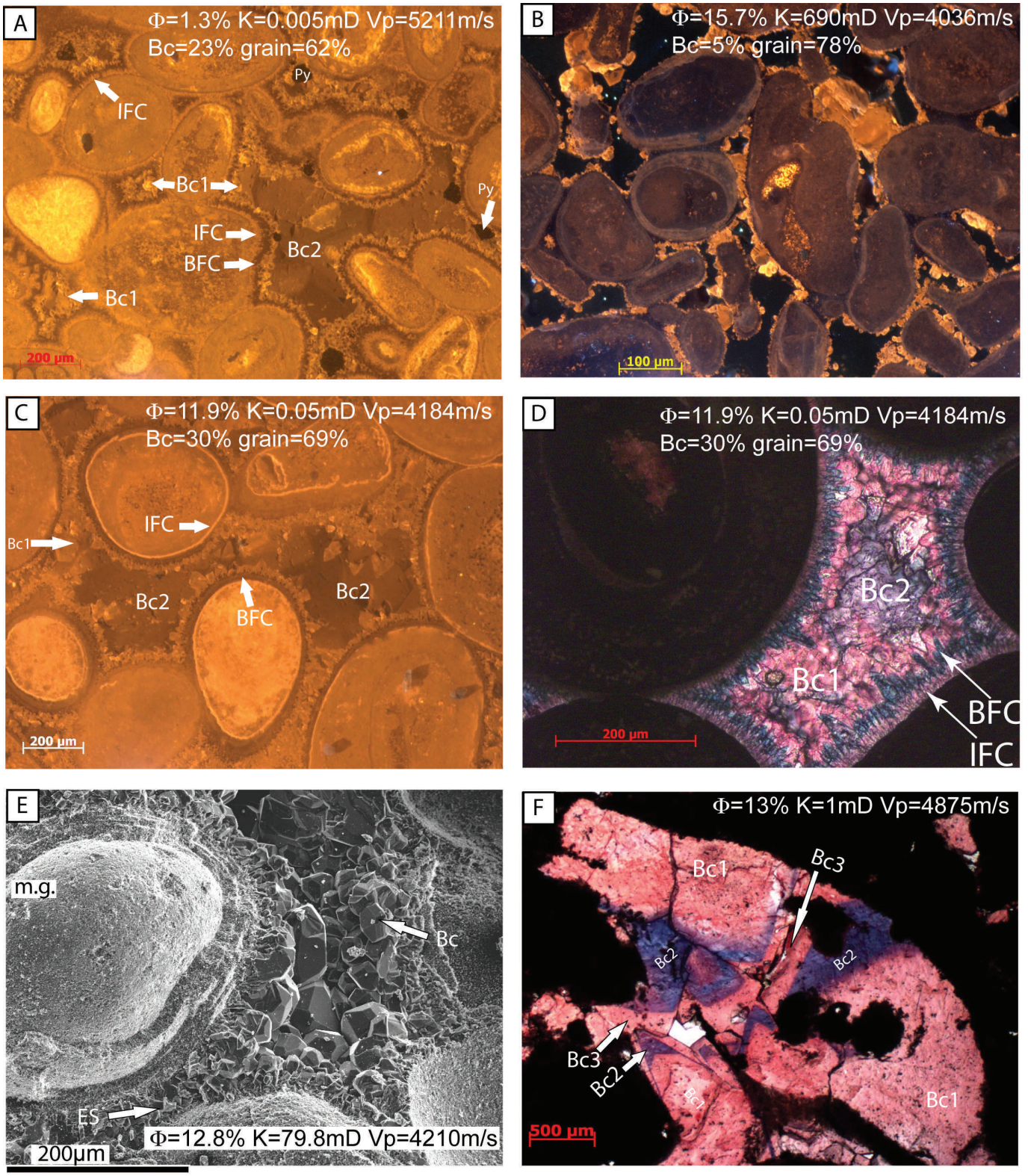

FIG. 7.—Photomicrographs of early and burial cements in the Middle Jurassic limestones. **A)** Cementation in ooid grainstone, isopachous fibrous cement (IFC), bladed ferroan calcite (BFC), blocky calcite 1 and 2 (Bc1 and Bc2), Oolite miliaire inférieure, E068 sample, EST210 core, 683 m. **B)** Meniscus cement in oolitic limestone. Note the limited blocky calcite development, Oolite de Fréville, E409 sample, EST433 core, 699.6 m. **C)** Cementation in ooid grainstone, IFC, BFC, Bc1, and Bc2, Oolite Miliaire, EST210 core, E078 sample, 689.5 m. **D)** Early cementation in ooid grainstone. IFC, BFC, Bc1, and Bc2, Oolite Miliaire, EST210 core, E078 sample, 689.5 m. **E)** Scanning electron microscope (SEM) observation in sample E413, Oolite de Fréville, 704 m, ooid is micritized, and porosity is partially filled by blocky calcite. **F)** Vug in ooid grainstone filled by the first (Bc1), second (Bc2), and third (Bc3) stages of blocky calcite, Calcaire de Chaumont, E028 sample, EST210 core, 649 m.

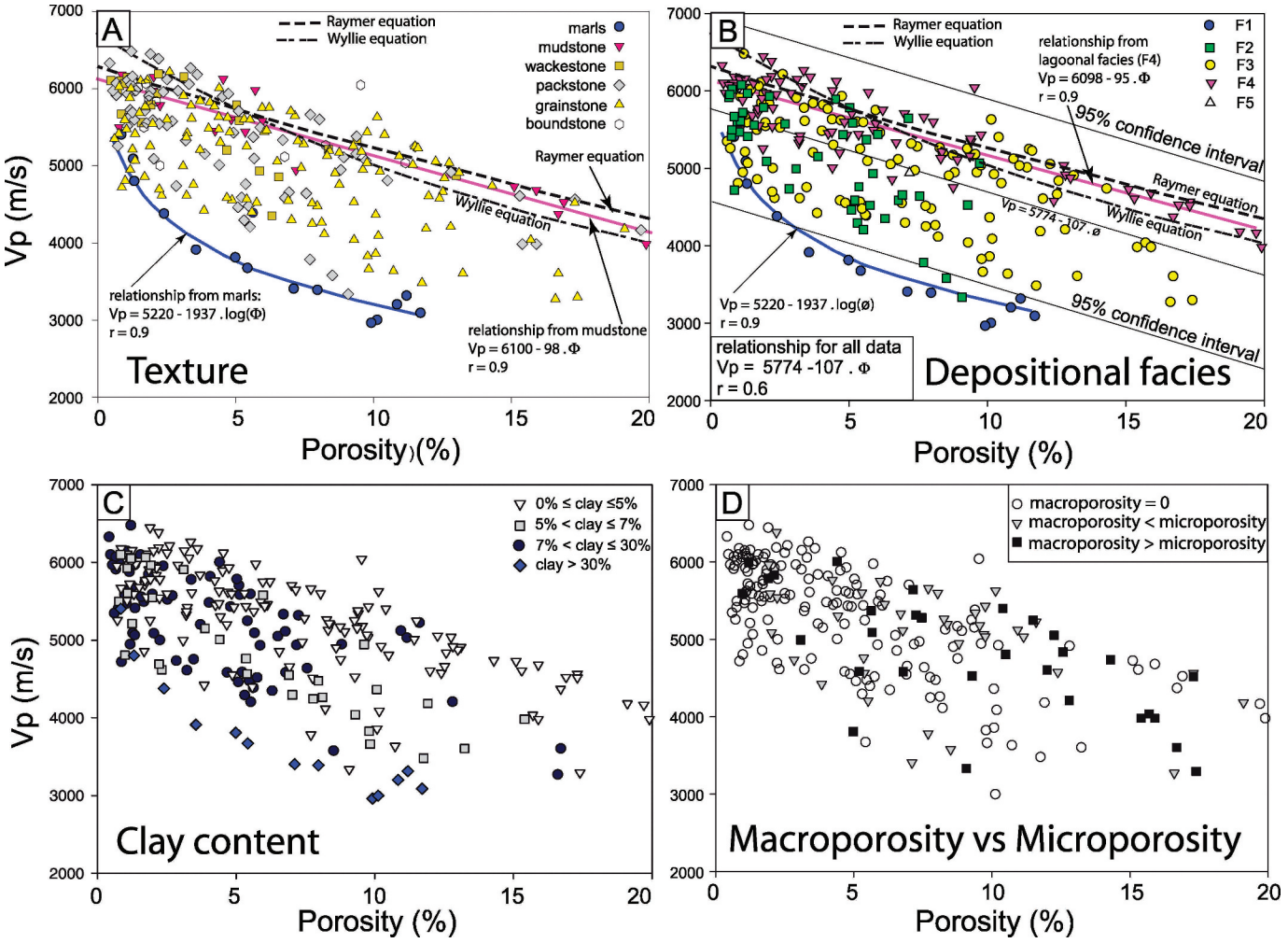

FIG. 8.—Velocity–porosity relationships from the Middle Jurassic limestones. **A)** Cross-plot of He porosity versus P-wave velocities from plug data in cores EST210, EST433 and HTM102. Data are sorted by texture (marls, mudstone, wackestone, packstone, grainstone, boundstone). **B)** Cross-plot of He porosity versus P-wave velocities from plug data in cores EST210, EST433, and HTM102. Data are sorted by facies. **C)** Cross-plot of He porosity versus P-wave velocities from plug data in cores EST210, EST433, and HTM102. Data are sorted by clay content (0–5%, 5–7%, 7–30%, > 30%). **D)** Cross plot of He porosity versus P-wave velocities from plug data in cores EST210, EST433, HTM102, and L.Li.CD.001. Data are sorted by porosity type (microporosity versus macroporosity).

from the southern border of the London–Brabant Massif, which was exposed and karstified during the uplifts of the Early Cretaceous (Thiry et al. 2006; Theveniaut et al. 2007). These two distinct paleohydrological circulation periods led to precipitation of blocky calcite in the captive phreatic aquifers, and are responsible for a marked reduction of porosity (from initially 40% to about 10%). The third zone of blocky calcite cement (Bc3) is related to Oligocene tectonic extension and fracturing (Buschaert et al. 2004; Brigaud et al. 2009b) which have a very limited influence on porosity (10% of the total cement volume). Currently, most of the studied limestones have porosity values lower than 10%. However, two porous levels (PL1 and PL2) with reservoir and aquifer properties occur in the upper part of Middle Jurassic sections (in Bathonian limestones), with porosity higher than 15%. For these porous layers, the occurrence of vadose cementation at the top of the PL1 and PL2 suggests a possible link with synsedimentary cementation and emersion, as in petroleum reservoirs of the Paris Basin (Purser 1978; Budd 1989). Early LMC meteoric cements and stabilization of metastable HMC in meteoric water during exposure periods rigidified the sediment, preventing compaction and pressure-solution processes, which restricted the potential source of carbonate for cementation and favored the preservation of the primary porosity in limestones (Purser 1978; Budd 1989; Alsharhan and Magara 1995; Volery et al. 2009, 2010). Determining the origin of highly porous levels is beyond the scope of this paper, and it is not discussed here.

Blocky calcite cements influence porosity and velocity in grainstone samples (Fig. 10A), yet in counterintuitive ways. For example, at porosity lower than 10%, the samples with a greater abundance of blocky calcite cement (above 20% of total volume) display lower velocity than samples with a lower proportion of blocky calcite contents (less than 20%; Fig. 10A). In fact, distinct porosity–velocity transforms are defined for those grainstones cemented early by isopachous fringes around grains and those non-early-cemented by isopachous fringes, only cemented by late blocky calcites after an early compaction stage (Fig. 10B). Discriminant analysis between early-cemented and early-compacted samples indicates a statistical difference, clearly forming two subsets (Fig. 10B).

These effects may be related to the timing of diagenesis, for at a given porosity, the lowest Vp are systematically associated with samples with early cement (Fig. 10B). Specifically, it appears that early cementation indurates the initial oo-bioclastic sands, making them more resistant to subsequent compaction. In these samples, the residual pore space is

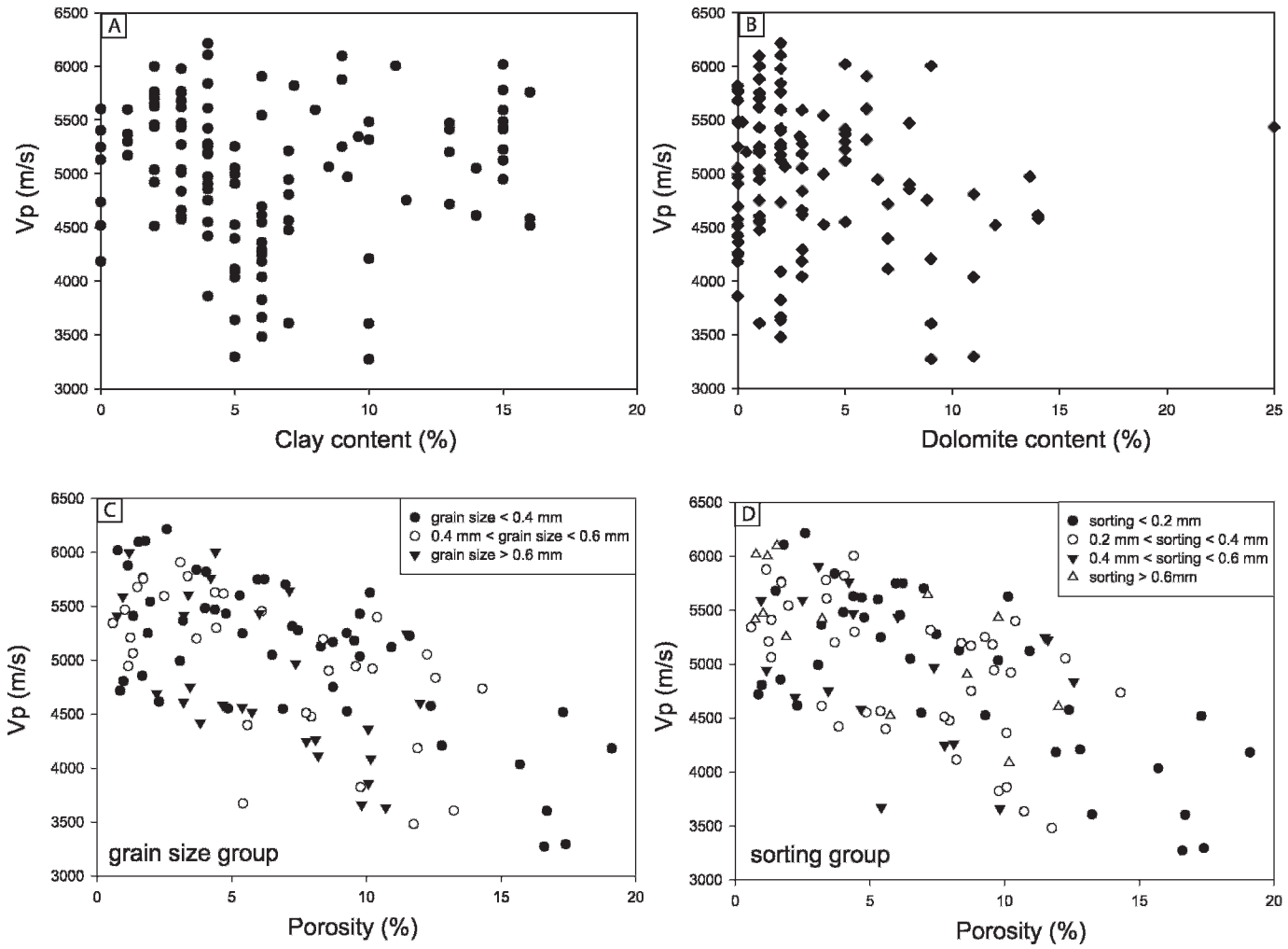

FIG. 9.—Velocity–porosity relationships from the grainstone samples of the Middle Jurassic limestones. **A)** Cross-plot of clay content versus P-wave velocities in grainstone samples only. **B)** Cross-plot of dolomite content versus P-wave velocities in grainstone samples only. **C)** Cross-plot of He porosity versus P-wave velocities from grainstone plug data in cores EST210, EST433, HTM102, and L.Li.CD.001. Data are sorted by grain size (< 0.4 mm, 0.4 mm to 0.6 mm, and > 0.6 mm). **D)** Cross-plot of He porosity versus P-wave velocities from grainstone samples in cores EST210, EST433, HTM102, and L.Li.CD.001. Data are sorted by sorting group (standard deviation of grain size; sorting < 0.2 mm, sorting between 0.2 mm and 0.4 mm, sorting between 0.2 mm and 0.4 mm, and > 0.6 mm).

cemented by at least two of the three successive blocky calcite cements (Brigaud et al. 2009b).

In contrast, poorly or later cemented grainstones mechanically compacted and experienced pore space reduction. In these rocks, ooids and/or bioclasts are generally micritized (Fig. 7). The early-compacted grainstone is thus volumetrically dominated by micrite (micritic ooids and micritic bioclasts), whereas the early-cemented grainstone, even though dominated by micrite (micritic ooids and micritic bioclasts), displays a much lower micrite/cement volume ratio (Fig. 10C).

Two distinct rock fabrics are defined in the grainstone dataset: (1) grainstone affected by early cementation (velocity transform: $Vp = 5222–84\phi$; $r = 0.6$), and (2) compacted grainstone with grain to grain contact (velocity transform: $Vp = 5968–98\phi$, $r = 0.8$). The subset affected by early cementation plots below the trend predicted by the Wyllie and Raymer time-average equations (Fig. 10B), and these standard time-average equations fail to predict the early cementation effect on sonic velocity (Fig. 10B). By contrast, the standard Wyllie and Raymer equations fit very well with the linear regression between porosity and velocity from early-compacted grainstones (Fig. 10B).

Porosity–Velocity Evolution through Diagenesis: From the Case Study to General Concepts.—The porosity–velocity cross-plot of grainstone illustrates the current stage of rock evolution. However, keeping in mind the distinct trends described above, i.e., early-cemented versus compacted grainstone, this cross-plot can also be interpreted as illustrating the evolution of the porosity and velocity during diagenesis with various fabrics reflecting variable degrees of diagenesis and two major diagenetic trajectories.

At deposition, oolitic and bioclastic sand includes about 40% porosity and velocity around 3000 m/s (Lucia 2007; Zinszner and Pellerin 2007) (Fig. 11A). There are two possible diagenetic pathways: early cementation and early compaction. In the case in which the oo-bioclastic sand was cemented immediately after sedimentation, this cement reduced porosity, from 40% to 15–20%, and thus also tended to raise Vp slightly (Fig. 11B). The remaining pore space was then cemented by burial cements, with the exception of the grainstone of the porous level PL1. The complete cementation by extensive blocky calcite(s) reduced porosity to 0–5%, and a coeval increase of Vp to 4500–5000 m/s (Fig. 11C, D).

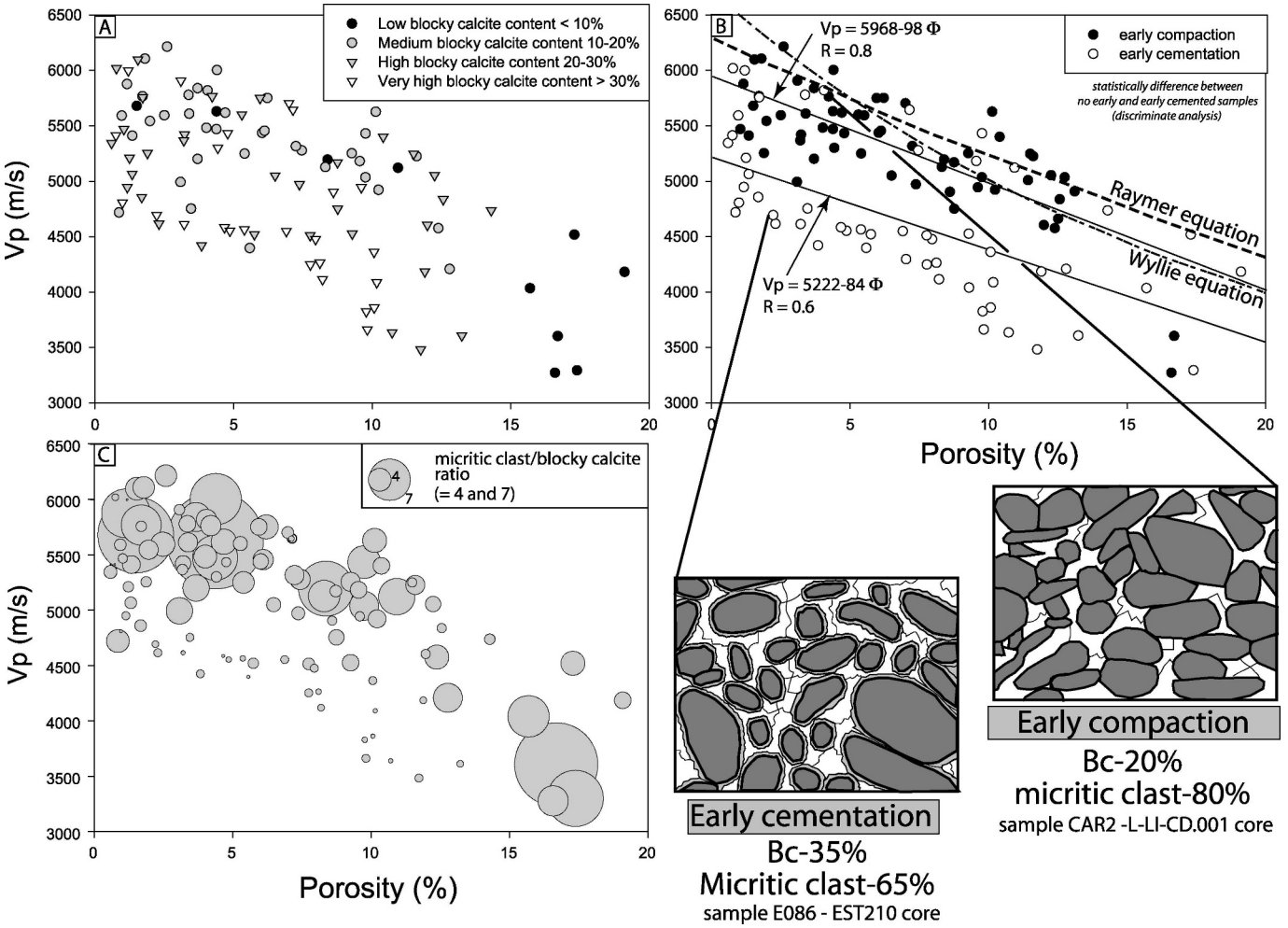

FIG. 10.—Influence of cements in velocity–porosity relationships. **A)** Cross-plot of He porosity versus P-wave velocities from grainstone samples in cores EST210, EST433, HTM102, and L.Li.CD.001. Data are sorted by blocky calcite content (low, medium, high, and very high). **B)** Cross plot of He porosity versus P-wave velocities from grainstone samples in cores EST210, EST433, HTM102, and L.Li.CD.001. Data are sorted by presence of early cement. The velocity transform is different between grainstone samples with and without early cementation. **C)** Cross-plot of He porosity versus P-wave velocities from grainstone samples in cores EST210, EST433, HTM102, and L.Li.CD.001. Data are sorted by micrite (micritic ooids and micritic bioclasts)/blocky calcite ratio (bubble size proportional to ratio).

In contrast, in the case in which no early cementation occurred, compaction would have caused grain-to-grain contacts and suturing, essentially forming a second diagenetic pathway (Fig. 11E–G). This compaction resulted in a grain-to-grain rock fabric (Fig. 11E), with porosity and Vp are 15–20% and 5000 m/s (as described in young limestones by Kenter 2002). These compacted samples had lower permeability, and so after limited burial cementation (5–10% of the rock volume) in the remaining pore space, acoustic velocities increased slightly to about 5500 m/s despite a porosity of 10% (Fig. 11F). After complete cementation, the velocities reached the highest values of the dataset (up to 6000 m/s; Fig. 11G), probably because the micritic network formed a relatively homogeneous physical medium without interfaces or discontinuities, favoring wave propagation (Fig. 11E–G).

Early Cementation and Rock Fabric.—The explanation for the two distinct trends is interpreted to be related to the evolution of the media during diagenesis, and to wave attenuation and velocity dispersion by diffraction (Bourbié et al. 1986; Zinszner and Pellerin 2007). In the first diagenetic phase, the decline in porosity with compaction and early cementation was the primary cause of Vp increase. However, for a similar porosity, this increase is less pronounced in early-cemented grainstone than in compacted grainstone. The compacted grainstone displays a continuous micritic network, favoring compressional wave propagation, whereas the early-cement fringes prevent such continuity, creating interfaces with micritic grains. On the contrary, due to the early cement connected pores inhibit development of a rigid micritic grain structure, favoring lower Vp. The first burial cements may not greatly modify the Vp, unless they markedly or completely fill pore space in the early-cemented grainstone. However, the early-cemented grainstone remains very heterogeneous, compared with the compacted grainstone, possibly including: (1) micritized grains (the structure of which depends on both the initial grain and the micritization process and degree), (2) early calcite fringes (the structure of which is also variable, fibrous and bladed for instance), and (3) burial calcite cements. These abundant interfaces between micritized grains, early calcite fringes, and blocky calcite cements may favor dispersion and wave attenuation, which could explain lower Vp than for the compacted grainstone with a continuous micritic network.

In sum, the data and interpretations suggest that the earliest diagenesis controls subsequent changes in pore and matrix structure, and hence porosity evolution and velocity, through the entire diagenetic history of

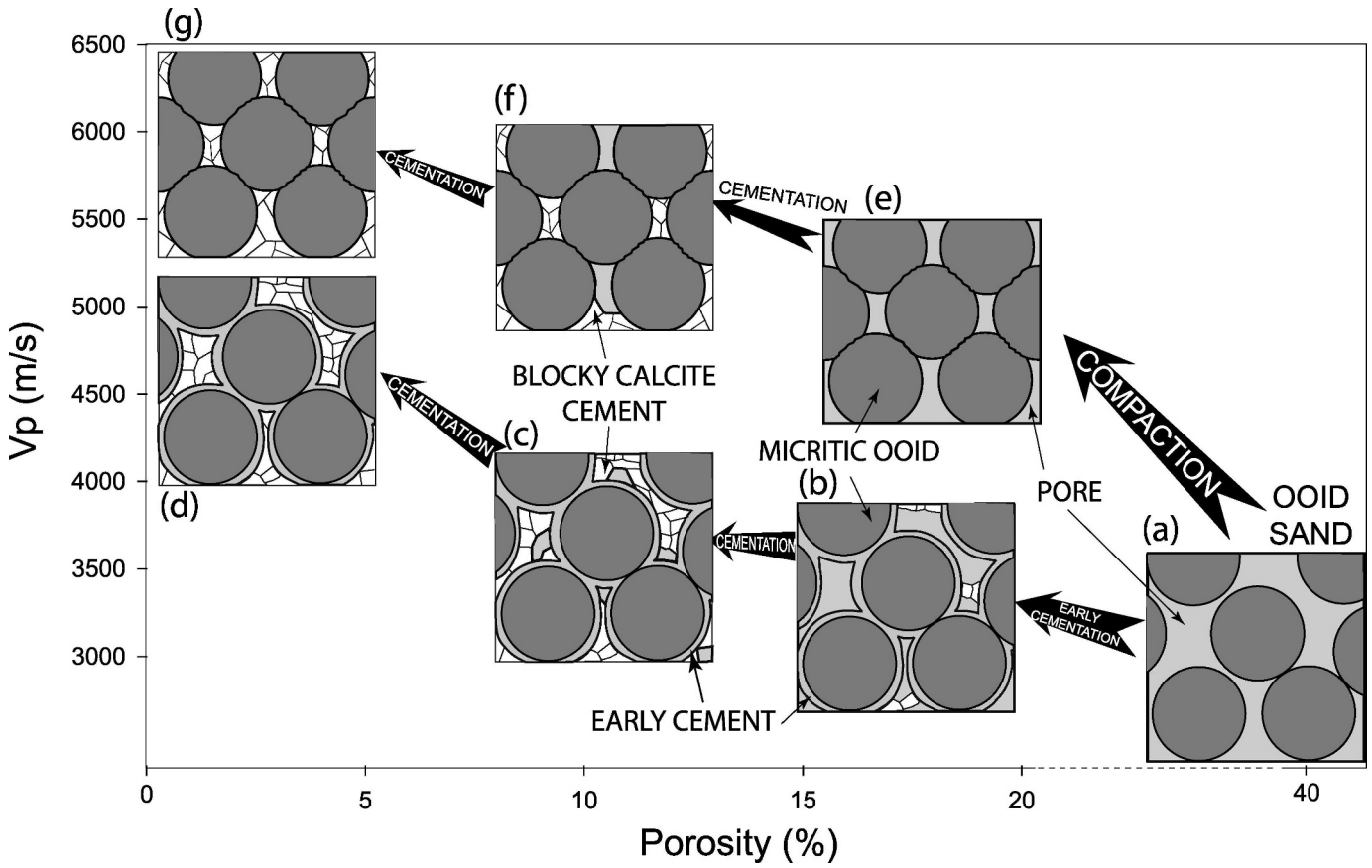

FIG. 11.—Velocity–porosity diagenetic trajectories in carbonate grainstones. Early cementation induces a different frame path compared to early-compacted grainstone. Two distinct diagenetic trajectories can be described from an initial point (a: ooid deposit): (1) grainstone rock fabric with early cement (b–c–d) and (2) grainstone rock fabric without early cement (e–f–g).

these carbonates (Anselmetti and Eberli 1993, 2001; Kenter et al. 2002). These earliest modifications explain the pronounced scatter of grainstone samples on the porosity–Vp cross-plots.

Velocity–Porosity Transforms in the Middle Jurassic Carbonate

Empirical equations for porosity–velocity transformation are provided in the literature (Wyllie et al. 1956, 1958; Gardner et al. 1974; Raymer et al. 1980), and can be used to predict porosity using inversion from seismic data. However, these relationships are far too general to be used blindly in every case study (Anselmetti and Eberli 1993; Kenter et al. 1997a; Anselmetti and Eberli 2001; Kenter et al. 2002; Lucia 2007). The detailed investigation of Middle Jurassic limestones of the Paris Basin presented here illustrates the distinctive controlling roles exerted by depositional environment and diagenesis on the details of the nature of the porosity–velocity transform. These two factors (depositional environment and diagenesis) summarize several possible factors that influence the porosity–velocity transform (texture, microporosity, macroporosity, early cementation, or meteoric-water input on grainstone and mudstone) (Fig. 12), which are likely to be distinct in many successions.

For porosity exceeding 15%, two distinct velocity domains occur. The higher velocities correspond to the microporous mud-lagoonal facies of porous level PL2 (Fig. 12). The presence of vadose cements at the top of the PL2 indicates an influence of local exposure during the Bathonian (see above). Above 15% porosity, the lower velocities correspond to the macroporous grainstone of the porous level PL1 (Fig. 12). Here again, exposure at the top of the interval promoted early vadose cementation and early mineral stabilization, limiting mechanical and chemical compactions. These two porous levels correspond to the intervals with highest formation water flux in the wells drilled by the Andra (transmissivity: 10^{-4} to 10^{-7}m^2/s; Scholz and Garry 2009). A porosity cutoff of 15% may then represent with potential aquifer zones. In this domain ($\phi > 15\%$ and Vp < 5000 m/s), two distinct velocity domains could be defined depending on the pore type involved. This point is key for the Andra, which might easily use these transforms to calculate the porosity of the porous levels and predict their distribution from seismic data.

CONCLUSIONS

Petrophysical examination of the Middle Jurassic carbonates of the Paris Basin, France, reveals several intriguing results. In this succession, mudstones and marls define two clear velocity–porosity transforms (Vp = 6100–98(ϕ); r = 0.9 and Vp = 5220–1937 log (ϕ)). The standard Wyllie and Raymer transforms fit very well with the linear regression between porosity and velocity from mudstone texture or lagoonal facies. These existing velocity transforms predict the acoustic velocities of muddy lagoonal facies relatively well.

In contrast, the velocities in microporous mudstone–wackestone of lagoonal facies are greater than in macroporous grainstone samples, at a given porosity range (15–20%) and grainstones display a wide range of both porosity and velocity. This large velocity variation in grainstone cannot be explained by variation of sorting, grain size, dolomite content

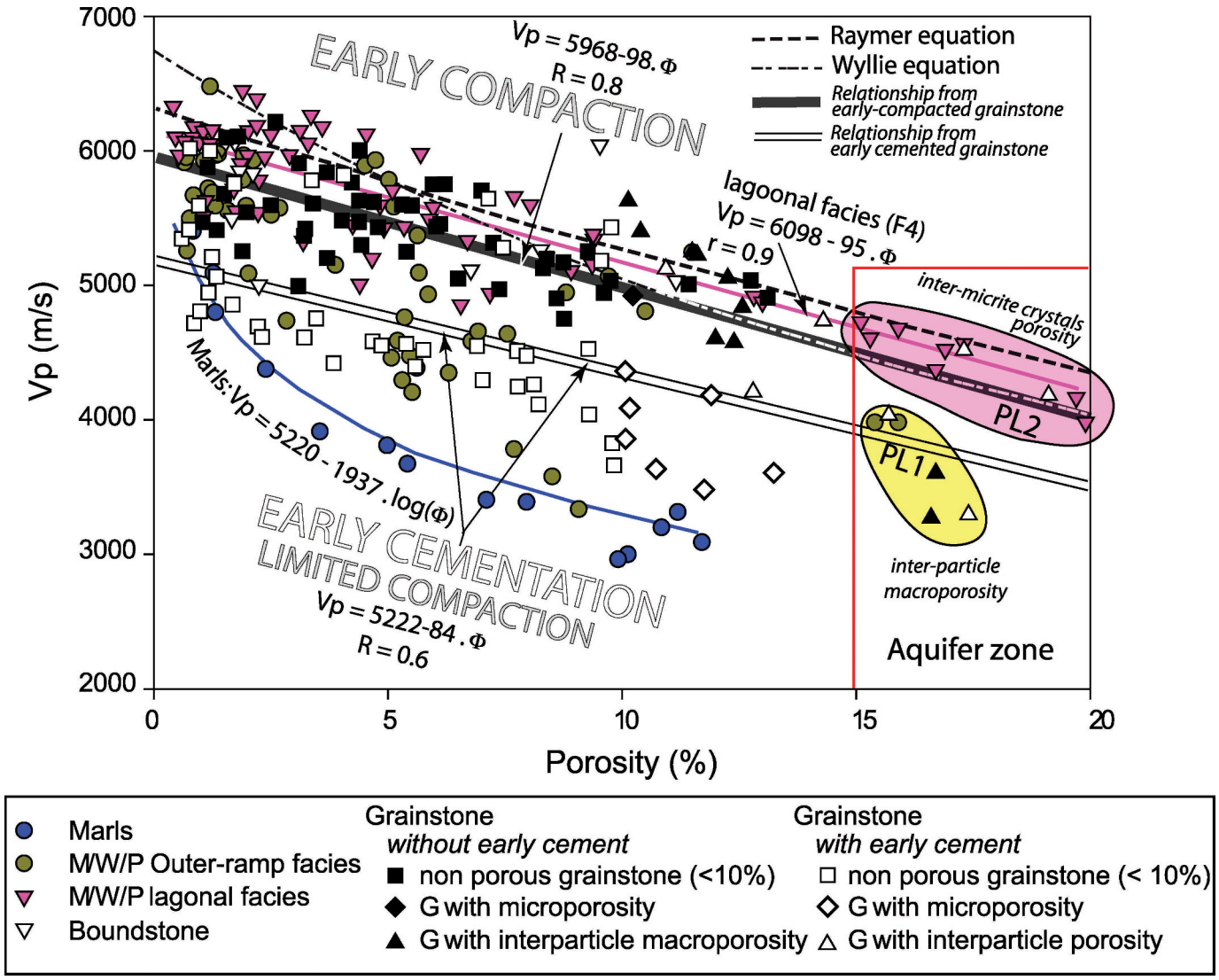

FIG. 12.—Velocity–porosity distribution in samples of carbonate environments. Early-cemented strata, early-compacted strata, lagoonal facies, and marls are clearly distinguished.

or clay content. Instead, early cementation plays an important role in acoustic velocity variation in grainstone. Early cements limit mechanical compaction, preserving a continuous macroporous network. Conversely, lack of early cementation favors mechanical compaction with grain-to-grain contacts, creating a continuous network which favors wave propagation (Vp = 5968–98(ϕ); r = 0.8). As such, the standard Wyllie and Raymer equations fit this linear regression from compacted grainstones. Where completely cemented during burial, the homogeneity of the micrite network formed by compacted micritic particles is preserved; in contrast, early-cemented grainstone is extremely heterogeneous, and includes non-touching grains, presence of isopachous fringe around grains, and blocky calcite cement. Such heterogeneity, with multiple interfaces and propagation media, favors diffraction and P-wave attenuation. As a result, the linear regression from early cemented grainstone (Vp = 5222–84(ϕ); r = 0.6) plots below the trend predicted by the Wyllie and Raymer time-average equations. Consequently, at a given porosity, velocities in compacted grainstone without early cementation are higher than in early-cemented grainstone. These results provide insights for the interpretation of Vp and the definition of transforms in grainstone bodies that could be applied to better understand seismic-based exploration and more accurately predict porosity in other carbonate successions.

ACKNOWLEDGMENTS

This study was supported by an Andra (French Agency for radioactive waste management) Ph.D. grant. We thank Christophe Auvray for allowing us to use ultrasonic equipment at LAEGO Laboratory (Nancy). TOTAL kindly authorized access to the L.LI.CD.1 core (we are especially grateful to Catherine Javaux, Guy Nesen, and Daniel Monge; Boussens site). Bernard Zinszner is thanked for constructive discussions on acoustic velocity. Jerry Lucia, Ralf Weger, Associate Editor Stacy Lynn Reeder, and Editor Eugene Rankey provided useful and constructive comments that improved an earlier version of this manuscript. The Appendix is available from the JSR Data Archive: http://www.sepm.org/jsr/jsr_data_archive.asp.

REFERENCES

ALSHARHAN, A., AND MAGARA, K., 1995, Nature and distribution of porosity and permeability in Jurassic carbonate reservoirs of the Arabian Gulf basin: Facies, v. 32, p. 237–253.

Anselmetti, F.S., and Eberli, G.P., 1993, Controls on sonic velocity in carbonates: Pure and Applied Geophysics, v. 141, p. 287–323.

Anselmetti, F.S., and Eberli, G.P., 2001, Sonic velocity in carbonates—a combined product of depositional lithology and diagenetic alteration, *in* Ginsburg, R.N., ed., Subsurface Geology of a Prograding Carbonate Platform Margin, Great Bahama Bank: Results of the Bahamas Drilling Project, SEPM, Special Publication 70, p. 193–216.

Anselmetti, F.S., von Salis, G.A., Cunningham, K.J., and Eberli, G.P., 1997, Acoustic properties of Neogene carbonates and siliciclastics from the subsurface of the Florida Keys: implications for seismic reflectivity: Marine Geology, v. 144, p. 9–31.

Assefa, S., McCann, C., and Sothcott, J., 1999, Attenuation of P- and S-waves in limestones: Geophysical Prospecting, v. 47, p. 359–392.

Assefa, S., McCann, C., and Sothcott, J., 2003, Velocities of compressional and shear waves in limestones: Geophysical Prospecting, v. 51, p. 1–13.

Baechle, G.T., Colpaert, A., Eberli, G.P., and Weger, R.J., 2008, Effects of microporosity on sonic velocity in carbonate rocks: The Leading Edge, v. 27, p. 1012–1018.

Bashore, W.M., Araktingi, U.G., Levy, M., and Schweller, W.G., 1994, Importance of a geological framework and seismic data integration for modeling and subsequent fluid-flow predictions, *in* Yarus, J.M., and Chambers, R.L., eds., Principles, Methods and Case Studies in Stochastic Modeling and Geostatistics, American Association of Petroleum Geologists 3, p. 159–176.

Bourbié, T., Coussy, O., and Zinszner, B., 1986, Acoustique des milieux poreux: Publication de l'Institut Français du Pétrole, 27, Technip, 339 p.

Braaksma, H., Proust, J.N., Kenter, J.A.M., Drijkoningen, G.G., and Filippidou, N., 2006, Sedimentological, petrophysical, and seismic characterization of an Upper Jurassic shoreface-dominated shelf margin (the Boulonnais, northern France): Journal of Sedimentary Research, v. 76, p. 175–199.

Brigaud, B., Durlet, C., Deconinck, J.-F., Vincent, B., Pucéat, E., Thierry, J., and Trouiller, A., 2009a, Facies and climate/environmental changes recorded on a carbonate ramp: A sedimentological and geochemical approach on Middle Jurassic carbonates (Paris Basin, France): Sedimentary Geology, v. 222, p. 181–206.

Brigaud, B., Durlet, C., Deconinck, J.-F., Vincent, B., Thierry, J., and Trouiller, A., 2009b, The origin and timing of multiphase cementation in carbonates: Impact of regional scale geodynamic events on the Middle Jurassic limestones diagenesis (Paris Basin, France): Sedimentary Geology, v. 222, p. 161–180.

Budd, D.A., 1989, Micro-rhombic calcite and microporosity in limestones: A geochemical study of the Lower Cretaceous Thamama Group, U.A.E: Sedimentary Geology, v. 63, p. 293–311.

Buschaert, S., Fourcade, S., Cathelineau, M., Deloule, E., Martineau, F., Ayt Ougougdal, M., and Trouiller, A., 2004, Widespread cementation induced by inflow of continental water in the eastern part of the Paris basin: O and C isotopic study of carbonate cements: Applied Geochemistry, v. 19, p. 1201–1215.

Contini, D., and Mangold, C., 1980, Evolution paléogéographique de la France au Jurassique moyen, *in* Enay, R., and Mangold, C., eds., Synthèse Paléogéographique du Jurassique Français: Document Laboratoire de Géologie de Lyon, v. 5, p. 66–70.

Durlet, C., and Thierry, J., 2000, Modalités séquentielles de la transgression aaléno–bajocienne sur le sud-est du Bassin parisien: Bulletin de la Société Géologique de France, v. 171, p. 327–339.

Enay, R., and Mangold, C., 1980, Synthèse paléogéographique du Jurassique français: Document du Laboratoire de Géologie de Lyon, v. 5, Groupe Français d'Etude du Jurassique, 220 p.

Fournier, F., and Borgomano, J., 2009, Critical porosity and elastic properties of microporous mixed carbonate–siliciclastic rocks: Geophysics, v. 74, p. E93–E109.

Gardner, G.H.F., Gardner, L.W., and Gregory, A.R., 1974, Formation velocity and density—the diagnostic basics for stratigraphic traps: Geophysics, v. 39, p. 770–780.

Gaumet, F., Garcia, J.P., Dromart, G., and Sambet, G., 1996, Stratigraphic control upon depositional facies, geometries and profiles across the Bathonian–Callovian carbonate platform in Burgundy: Bulletin de la Société Géologique de France, v. 167, p. 409–421.

Gaumet, F., Garcia, J.P., Dromart, G., and Allemand, P., 2001, Middle Jurassic production rates and "patchy" architecture of the carbonate systems along the north-western Tethyan margin (Paris basin to Sub-alpine basin): Géologie Méditerranéenne, v. 25, p. 79–83.

Granier, B., 1995, A sedimentological model of the Callovian oolite reservoir of the Villeperdue oil field, Paris Basin (France): Petroleum Geoscience, v. 1, p. 145–150.

Guillocheau, F., Robin, C., Mettraux, M., Dagallier, G., Robin, F.-X., and Le Solleuz, A., 2002, Le Jurassique de l'Est du Bassin de Paris: Bulletin Information des Géologues du Bassin Paris, v. 39, p. 23–47.

Kenter, J.A.M., and Ivanov, 1995, Parameters controlling acoustic properties of carbonate and siliclastic sediments at Sites 866 and 869, *in* Winterer, E.L., Sager, W.W., Firth, J.V., and Sinton, J.M., eds., Proceedings of the Ocean Drilling Program, Initial Scientific Results, College Station, Texas, Ocean Drilling Program, v. 143, p. 287–303.

Kenter, J.A.M., Fouke, B.W., and Reinders, M., 1997a, Effects of differential cementation on the sonic velocities of Upper Cretaceous skeletal grainstones (southeastern Netherlands): Journal of Sedimentary Research, v. 67, p. 178–185.

Kenter, J.A.M., Podladchikov, F.F., Reinders, M., Van der Gaast, S.J., Fouke, B.W., and Sonnenfeld, M.D., 1997b, Parameters controlling sonic velocities in a mixed carbonate–siliciclastic Permian shelf-margin (upper San Andres formation, Last Chance Canyon, New Mexico): Geophysics, v. 62, p. 505–520.

Kenter, J.A.M., Gartner, G.L.B., and Schlager, W., 2001, Seismic models of a mixed carbonate–siliciclastic shelf margin: Permian upper San Andres Formation, Last Chance Canyon, New Mexico: Geophysics, v. 66, p. 1744–1748.

Kenter, J.A.M., Anselmetti, F.S., Kramer, P.H., Westphal, H., and Vandamme, M.G.M., 2002, Acoustic properties of "young" carbonate rocks, ODP leg 166 and boreholes Clino and Unda, western Great Bahama Bank: Journal of Sedimentary Research, v. 72, p. 129–137.

Kenter, J.A.M., Braaksma, H., Verwer, K., and van Lanen, X.M.T., 2007, Acoustic behavior of sedimentary rocks: Geologic properties versus Poisson's ratios: The Leading Edge, v. 26, p. 436–444.

Lambert, L., Durlet, C., Loreau, J.-P., and Marnier, G., 2006, Burial dissolution of micrite in Middle East carbonate reservoirs (Jurassic–Cretaceous): Keys for recognition and timing: Marine and Petroleum Geology, v. 23, p. 79–92.

Loreau, J.P., 1972, Petrographie des calcaires fins au microscope electronique à balayage: introduction à une classification des micrites: Comptes Rendus Hebdomadaires des Séances de l'Academie des Sciences (Paris), v. 274, p. 810–813.

Lucia, J.F., 2007. Carbonate Reservoir Characterization, Second Edition: Berlin, Springer-Verlag, 336 p.

Melzer, S.E., and Budd, D.A., 2008, Retention of high permeability during shallow burial (300 to 500 m) of carbonate grainstones: Journal of Sedimentary Research, v. 78, p. 548–561.

Menjoz, A., Brach, M., Criaud, A., Fouillac, C., Lambert, M., and Rojas, J., 1992, Caractérisation et modélisation du réservoir géothermique du Dogger (Bassin Parisien): Géochronique, v. 43, p. 20–21.

Mougenot, D., 1999, Seismic imaging of a carbonate reservoir: the Dogger of the Villeperdue oil field, Paris Basin, France: Petroleum Geoscience, v. 5, p. 75–82.

Purser, B.H., 1967, Le Comblanchien—Interprétation de son milieu de sédimentation: Revue de l'Institut Français du Petrole et Annales des Combustibles Liquides, v. 22, p. 591–594.

Purser, B.H., 1975, Sédimentation et diagenèse précoce des séries carbonatées du Jurassique moyen de Bourgogne [unpublished Thesis]: Orsay, 450 p.

Purser, B.H., 1978, Early diagenesis and the preservation of porosity in Jurassic limestones: Journal of Petroleum Geology, v. 1, p. 83–94.

Purser, B.H., 1989. Plates-formes carbonatées exemple du Jurassique moyen du Bassin de Paris, Dynamique et méthodes d'étude des bassins sédimentaires, Technip, p. 145–164.

Rafavich, F., Kendall, C.H.S.C., and Todd, T.P., 1984, The relationship between acoustic properties and the petrographic character of carbonate rocks: Geophysics, v. 49, p. 1622–1636.

Raymer, D.S., Hunt, E.R., and Gardner, J.S., 1980, An improved sonic transit time-to-porosity transform: Presentation at the Society of Professional Well Log Analysts: 21st Annual Meeting, p. 1–12.

Robinson, A., Griffiths, C., Price, S., Hegre, J., and Muggeridge, A., 2008, The Future of Geological Modeling in Hydrocarbon Development: The Geological Society of London, Special Publiction, v. 309, 226 p.

Roduit, N., 2008, JMicroVision: Image analysis toolbox for measuring and quantifying components of high-definition images. Version 1.2.7. http://www.jmicrovision.com (accessed march 2009).

Røgen, B., Fabricius, I.L., Japsen, P., Høier, C., Mavko, G., and Pedersen, J.M., 2005, Ultrasonic velocities of North Sea chalk samples: influence of porosity, fluid content and texture: Geophysical Prospecting, v. 53, p. 481–496.

Scholz, E., and Garry, B., 2009, Mise en relation des données hydrogéologiques et géologiques sur les encaissants: Apport de la campagne FZT, Andra, 39 p.

Sterpenich, J., Sausse, J., Pironon, J., Gehin, A., Hubert, G., Perfetti, E., and Grgic, D., 2009, Experimental aging of oolitic limestones under CO_2 storage conditions: Petrographical and chemical evidence: Chemical Geology, v. 265, p. 99–112.

Theveniaut, H., Quesnel, F., Wyns, R., and Hugues, G., 2007, Palaeomagnetic dating of the "Borne de Fer" ferricrete (NE France): Lower Cretaceous continental weathering: Palaeogeography, Palaeoclimatology, Palaeoecology, v. 253, p. 271–279.

Thierry, J., and Barrier, E., 2000, Middle Callovian, map 9, *in* Dercourt, J., Gaetani, M., Vrielynck, B., Barrier, E., Biju-Duval, B., Brunet, M.F., Cadet, J.P., Crasquin, S., and Sandulescu, M., eds., Atlas Peri-Tethys, Palaeogeographical Maps: Explanatory Notes, Commission de la Carte Géologique du Monde, Paris, p. 49–110.

Thiry, M., Quesnel, F., Yans, J., Wyns, R., Anne, V., Theveniaut, H., Simon-Coincon, R., Ricordel, C., Moreau, M.G., Giot, D., Dupuis, C., Bruxelles, L., Barbarand, J., and Baele, J.M., 2006, Continental France and Belgium during the early Cretaceous: paleoweatherings and paleolandforms: Bulletin de la Société Géologique de France, v. 177, p. 155–175.

Verwer, K., and Braaksma, H., 2009, Data report: petrophysical properties of "young" carbonate rocks (Tahiti Reef Tract, French Polynesia), *in* Camoin, G.F., Iryu, Y., Mclnroy, D.B., et al., eds., Proceedings of the Integrated Ocean Drilling Program, Washington, v. 310, p. 1–23.

Verwer, K., Braaksma, H., and Kenter, J.A.M., 2008, Acoustic properties of carbonates: Effects of rock texture and implications for fluid substitution: Geophysics, v. 73, p. B51–B65.

Vincent, B., Emmanuel, L., Houel, P., and Loreau, J.-P., 2007, Geodynamic control on carbonate diagenesis: Petrographic and isotopic investigation of the Upper Jurassic formations of the Paris Basin (France): Sedimentary Geology, v. 197, p. 267–289.

Volery, C., Davaud, E., Foubert, A., and Caline, B., 2009, Shallow-marine microporous carbonate reservoir rocks in the Middle East: relationship with seawater Mg/Ca ratio and eustatic sea level: Journal of Petroleum Geology, v. 32, p. 313–325.

Volery, C., Davaud, E., Foubert, A., and Caline, B., 2010, Lacustrine microporous micrites of the Madrid Basin (late Miocene, Spain) as analogues for shallow-marine carbonates of the Mishrif reservoir Formation (Cenomanian to Early Turonian, Middle East): Facies, v. 56, p. 385–397.

Weger, R.J., Eberli, G.P., Baechle, G.T., Massaferro, J.L., and Sun, Y.-F., 2009, Quantification of pore structure and its effect on sonic velocity and permeability in carbonates: American Association of Petroleum Geologists, Bulletin, v. 93, p. 1297–1317.

Wendebourg, J., and Lamiraux, C., 2002, Estimating the ultimate recoverable reserves of the Paris Basin, France: Oil and Gas Science and Technology—Revue de l'Insitut Français Pétrole, v. 57, p. 621–629.

Wyllie, M.R.J., Gregory, A.R., and Gardner, G.H.F., 1956, Elastic wave velocities in heterogeneous and porous media: Geophysics, v. 21, p. 41–70.

Wyllie, M.R.J., Gregory, A.R., and Gardner, G.H.F., 1958, An experimental investigation of factors affecting elastic wave velocities in porous media: Geophysics, v. 23, p. 459–493.

Zinszner, B., and Pellerin, F.-M., 2007, A geoscientist's guide to petrophysics: Insitut Français du Pétrole Publication, Technip, 384 p.

Received 24 July 2009; accepted 5 March 2010.